To the Graduate Council:

I am submitting herewith a thesis written by Maria Siopsis entitled "An Individual-Based Model for the Toxic Algae Species *Pseudo-nitzschia multiseries*". I have examined the final electronic copy of this thesis for form and content and recommend that it be accepted in partial fulfillment of the requirements for the degree of Doctor of Philosophy, with a major in Mathematics.

Thomas G. Hallam

Major Professor

We have read this thesis
and recommend its acceptance:

Louis J. Gross

Samuel Jordan

Steven Wilhelm

Accepted for the Council:

Anne Mayhew

Vice Provost
and Dean of Graduate Studies

(Original signatures are on file with official student records)

AN INDIVIDUAL-BASED MODEL FOR THE TOXIC ALGAE SPECIES *PSEUDO-NITZSCHIA MULTISERIES*

A Dissertation

Presented for the

Doctor of Philosophy Degree

The University of Tennessee, Knoxville

Maria Siopsis

May 2003

DEDICATION

To my families, Theoharidis, Karantanis and Siopsis who each in their own way are a part of who I am and what I have accomplished.

"'It's possible, but not interesting,' Lönnrot answered. 'You will reply that reality hasn't the slightest need to be of interest. And I'll answer you that reality may avoid the obligation to be interesting, but that hypothesis may not . . .'"

Jorge Luis Borges, Death and the Compass

Acknowledgements

First, I would like to thank my advisor Thomas G. Hallam, who has helped me through the scientific, professional, and personal obstacles I have met during this long process with intelligence, understanding and caring. He is special to me as an academic advisor and a life advisor. Without his help, this dissertation would not be a reality.

I must also acknowledge the contribution of the members of The Institute for Environmental Modeling. Thanks to my fellow graduate students who have helped me by listening to me talk about my work and by talking about other things important to life to keep everything in perspective. Special thanks also go to Louis Gross, who I admire as a scientist and a person. He has been an invaluable resource not only by answering my questions, but by asking me questions that forced me to think about my work in new ways.

Equally important to this work is Stephen Bates, whose knowledge of *Pseudo-nitzschia* species and his willingness to share it with me provided a constant source of information regarding the biology of the problem.

Thanks also to committee members Samuel Jordan and Steven Wilhelm. It was my pleasure to learn mathematics from a teacher like Dr. Jordan. He will serve as a model to me in my career as a college professor. Steven Wilhelm's expertise in the biology of algae has been much appreciated. I have valued our conversations about biology as they have helped shape the way the work presented here has developed.

I would like to acknowledge my parents, Dionysios and Eleni Theoharidis, who

have taken care of me and my family while I worked towards completing this task.

Thanks also to my colleagues at Maryville College, especially the Division of Mathematics. I appreciate their support as I went through the final stages of this dissertation. Their positive words have often lifted my spirits and rejuvenated my optimism.

Finally, thanks to Giorgos, my husband, who has been supportive and patient with me through this long process. I don't have words to express how much he means to me.

Abstract

In 1987 an outbreak of a previously unobserved disease occurred in Canada and was traced back to the toxin domoic acid produced by the diatom *Pseudo-nitzschia multiseries*. Since then, fisheries closures due to domoic acid have occurred worldwide. *Pseudo-nitzschia* species produce domoic acid under nutrient stress, including low silicon or phosphorus under high nitrogen conditions. However, it is still unclear what conditions cause the dangerously high levels that have sometimes been observed. We present an individual-based algae model detailing the physiology of an algal cell with a focus on nutrient and energy flows to delineate the causes of domoic acid production.

The model has been adapted to the specific problem of *Pseudo-nitzschia multiseries* by including silicon dynamics, a frustule component, domoic acid production, and sexual reproduction. The individual model is incorporated into a population model using a McKendrick-von Foerster partial differential equation.

The model is compared to experimental data from chemostat and batch experiments on two separate strains of *Pseudo-nitzschia multiseries*. The differences in parameter values required to fit each experiment reveal differences in the physiology of the two strains, specifically in nutrient uptake, photosynthetic rate and the level of toxin production possible. Simulations using the calibrated model show that silicon limitation must be concurrent with an abundance of nitrogen for domoic acid production to be high.

Contents

Chapter

Tables

Table

Figures

Figure

Chapter 1

Introduction: Biological background and model description

1.1 Harmful algae blooms and *Pseudo-nitzschia* species

Throughout history, coastal areas have dealt with large algal blooms called "red tides"; however, the past twenty years have been marked by a global increase in their frequency and distribution. Although the reasons for this increase have not been determined, there are several possible causative factors including higher nutrient content in water, atypical nutrient regimes and ratios due to cultural eutrophication, and ballast water redistribution [33].

Red tides are a subset of events known as "harmful algal blooms" (HAB's) because they may be deleterious to specific organisms and to ecosystems in general. *Pseudo-nitzschia multiseries*, of interest for this work, produces the neurotoxin domoic acid (DA) placing it in a category with fewer than 100 which are known to produce toxins out of approximately 5000 known algal species [33]. Since algae are primary producers in aquatic ecosystems, the presence of a toxin-producing species in a marine ecosystem can have repercussions for the entire food chain. Species of *Pseudo-nitzschia* have been implicated in poisonings of sea birds, large sea mammals, and humans [2, 30, 52].

The human health and economic effects caused by toxic algae are of major concern. Outbreaks have caused thousands of illnesses and several deaths. When an area suffers an outbreak, the local economy may lose millions of dollars in fishery revenues in addition to immeasurable losses in tourism. It is important therefore to attempt to

understand the ecosystems containing these algae.

1.2 *Pseudo-nitzschia multiseries* and Domoic Acid

In Canada during 1987 an outbreak of a previously unobserved disease occurred. Victims experienced typical symptoms of gastroentiritis coupled with neurological disorders including disorientation and memory loss. After investigation, the cause of the disease was traced to mussels harvested from Prince Edward Island and the disease was dubbed Amnesic Shellfish Poisoning (ASP). It was later determined that the toxin responsible for ASP is domoic acid, an amino acid produced by the diatom *Pseudo-nitzschia multiseries*. Mussels feeding on this diatom can accumulate sufficiently high levels of DA to render them toxic to humans and other animals that eat them. [74].

DA (Figure A.1) is an excitatory neurotoxic amino acid [25] which disrupts normal neurochemical transmission in the brain, causing increased firing of the neurons thereby destroying the cells [10]. The neurons in the hippocampus, the part of the brain most responsible for formation and storage of memories, are particularly affected by DA [42]. This explains the memory loss associated with ASP. In order to prevent further illness, guidelines have been set for DA and *Pseudo-nitzschia* concentrations. Human exposures of 1mg DA/kg mussel meat are considered dangerous [42]; therefore, any shellfish exceeding 20 mg DA/kg wet weight or tissue are considered unsuitable for consumption and shellfish beds are closed when the concentration of *Pseudo-nitzschia* cells exceeds 100,000 cells per Liter [6].

Since the 1987 incident in Canada, domoic acid has been detected in several worldwide locations, causing fishery closings and deaths of large marine mammals (Table B.1). This has sparked several studies into the characteristics and relationships between DA and *Pseudo-nitzschia* species. Chemists are attempting to characterize the

toxin while biologists have attempted to characterize the conditions under which it is produced. *Pseudo-nitzschia* are pennate, chain forming diatoms which can be motile [54]. They have been found in the coastal waters of the northeast United States, eastern Canada, the northwest United States, New Zealand, and Asia [6]. Due to the potential toxicity, their life cycle and environmental needs have been extensively studied.

1.2.1 Silicon, Life Cycle, and Environmental Conditions

One important difference between diatoms and other algal species is that their cell walls are enclosed within a silicon shell called a frustule. The requirements for creation of the frustule make diatoms uniquely dependent on the availability of silicon for continued growth. A lack of silicon can arrest the cell cycle in a stage between mitosis and daughter cell separation, a period of silicon uptake and deposition of the newly forming frustule [14, 71, 72]. It has also been shown that silicon is an important element in other diatom cell processes such as DNA replication and protein synthesis [71].

The frustule is composed of two interlocking halves, one larger than the other. This arrangement can be pictured as a hat box where the lid has a slightly larger diameter than the base. The larger piece is called the epitheca and the smaller is called the hypotheca. Once protoplasm cleavage is completed, the cells form two new hypothecae inside of the frustule of the parent cell. The result is one cell that is the same size as the parent cell and one cell that is slightly smaller. This continued process results in a reduction in the average cell size of the population. Sexual reproduction may occur, resulting in return of larger cells (Figure A.2) [12].

The same cycle occurs in *Pseudo-nitzschia multiseries*. The large cells that are the products of sexual reproduction continually divide resulting in successively smaller cells, until the cells reach a minimum size and begin reproducing sexually. *Pseudo-nitzschia multiseries* is a dioecious organism; therefore, both "male" and "female" cells

must be present for sexual reproduction to occur. Each cell produces two gametes, and each pair may produce either one or two auxospores that develop into full-sized cells probably through the use of nutrient reserves in the parent cells. Auxospores of *Pseudo-nitzschia multiseries* take an average of 48 hours to become fully developed cells [19]. It is likely that"younger" cells, i.e. those produced by sexual reproduction, are more toxic than older, smaller ones [6, 19].

Many have studied *Pseudo-nitzschia* species to characterize favorable environmental conditions. Pan and coworkers studied how light levels affect growth and cellular nitrogen (N), carbon (C), and chlorophyll a, as well as how the organism can adapt to low light levels [62, 60]. They also determined the photosynthesis - photosynthetic photon flux density (PPFD) relationship [60]. Jackson determined the salinity range tolerated by *Pseudo-nitzschia multiseries* to be between 15 and 48%, and the effect of salinity on maximum density and growth [43]. Bates and coworkers studied silicate and have found that there is a linear relationship between initial silicate concentration and cell yield in batch cultures [3]. There have also been studies that show the source of nitrogen affects growth. Cells that receive N from nitrate grow faster than those that use ammonium. In fact, ammonium in sufficient concentration can actually arrest cell growth [8, 36]. Bates et. al. [6] have characterized the effects of temperature on growth, photosynthesis, and DA production.

1.2.2 DA Production

DA production has also been the focus of many studies. According to Pan et. al. [58, 61] there are two stages of DA production. The first corresponds to the late exponential phase when the growth rate is slowing down after a period of rapid increase. The second is during the stationary phase when population growth ceases due to nutrient limitation. More DA is produced in the second stage than in the first [58, 61].

Production of DA is therefore probably triggered by some kind of stress, and is negatively correlated to growth rate [7]. There are five nutrients that play a role in DA production: nitrogen, silicon (Si), phosphorus (P) and the readily available elements carbon and hydrogen (H). If the population is N limited, DA production will not occur even though cells are no longer dividing [3]. On the other hand, sufficiently low levels of P or Si trigger production of DA. DA production is negatively correlated with both P and Si available in the system. However, production under silicate limitation is higher than production under phosphate limitation [58, 61].

Another factor determining DA production is the interaction of bacteria with the diatom. As with many other plants and bacteria, it appears there are symbiotic relationships between *Pseudo-nitzschia* species and their associated bacteria. It has been shown that non-axenic (bacteria-containing) cultures of *Pseudo-nitzschia* survive longer in the stationary phase than axenic cultures and that DA production can increase by 20% when bacteria are present in the system [22]. While growth rate and cell yield remained unaffected when bacteria were reintroduced to axenic cultures of *Pseudo-nitzschia multiseries*, DA production was 8 to 38 times higher than without bacteria. This range of production depends on the strain of algae used. Several different types of bacteria can cause this increase, regardless of whether they are originally isolated from toxic algal species or not [4, 5]. The reasons for the increase in DA production are not entirely understood; however, the bacteria may be producing a precursor to DA or providing dissolved organic matter or CO_2 which contain carbon and nitrogen for DA synthesis. It may also be that bacteria are responsible for regenerating nutrients which prolong the viability of algal cells during the stationary phase when DA is known to be produced [5, 22].

The most extensive work on the interaction of DA producing diatoms and bacteria has been done by Stewart [70]. He has isolated bacteria from several strains of DA producing diatoms. The bacteria that were isolated could be divided into two groups.

The first group is able to produce significant amounts of acids from carbohydrates. In particular, all cultures yielded at least one bacterial species that produced gluconic acid/gluconolactone from glucose. This substance is thought to be of importance in DA production. The second group were able to grow readily by using free amino acids. When bacteria were separated from the algae they were not able to divide or even grow well without a source of organic nitrogen. This implies that the diatom may provide organic nitrogen for the bacteria. On the other hand, the growth of non-axenic diatoms was increased by adding proline to the medium, but the addition did not affect the growth of axenic cultures. Because proline also aids in bacterial growth it is suggested that bacterial growth provides organic materials in the form of proteins, peptides and free amino acids each of which is a source of nitrogen-containing ammonium for the diatom [70].

Osada and Stewart [57] have studied the physiological influences of gluconic acid/gluconolactone on DA production. By adding substances to axenic and non-axenic diatom cultures they have obtained some interesting results. Specifically, the highest rate of DA production was observed in an axenic culture when gluconic acid/gluconolactone was added to the medium. Moreover, the effect of this substance on DA production is concentration dependent, with higher concentrations of gluconic acid/gluconolactone resulting in generally higher production of DA. Additionally, DA production was enhanced by the presence of a gluconic acid/gluconolactone-producing bacterium but not in the presence of a non-producer. It is hypothesized that since gluconic acid/gluconolactone can act as a sequestering agent, the increase in DA production is due to more severe nutrient limitation when it is present.

1.3 Existing HAB Models

As early as 1953, models were used to study algal blooms. The Kierstead and Slobodkin model [**?**] examined the opposing effects of growth rate and diffusion on

phytoplankton blooms. This model consists of one algal species exhibiting a linear growth rate which is limited physically by diffusion out of a favorable patch of water. It is represented by the following equation:

$$\frac{\partial c}{\partial t} = D\frac{\partial^2 c}{\partial x^2} + Kc \tag{1.1}$$

where c is the concentration of algae (cells/unit length), D (length^2/time) is the diffusivity, K is the growth rate(time^{-1}) per unit population, t is time and x is the horizontal position. At the boundaries $x = 0$ and $x = L$, c is set to zero, representing unfavorable conditions outside the patch. The model is then used to quantify a minimum patch length, L, related to the ratio of diffusion to growth, that can maintain a bloom [48]. Since the advent of reaction-diffusion problems, other models have been developed with different goals in mind [29].

The simplest of these other models are the aggregated ones without complex physical dynamics such as currents, shear, and mixing. For example, Wyatt and Horwood [77] considered a dinoflagellate species with motile and non-motile components, both subject to constant grazing pressure. By assuming that the water is well stratified and that the motile algae choose to congregate at the depth where their reproductive rate is maximized, the authors conclude that red tides can result when water is stratified allowing motile red tide organisms to move to the water depth that is most favorable to them and thus escape control by grazers. The authors include toxin levels using the concentration of the algae coupled with diffusivity [77].

Another example of an aggregated model is that of Truscott [75] which includes a phytoplankton species and a grazer in a homogeneous environment. The phytoplankton grow logistically according to nutrient limitation and the grazers have constant mortality. Efficiency of metabolism and handling times for the grazers are also included. Truscott treats this as an excitable system, such that small changes in specific phyto-

plankton growth rate can allow the phytoplankton to escape grazer control and form a bloom.

While aggregated models give an idea of phytoplankton dynamics, they consider a system of only one algal species when often there are several species present in a bloom. Researchers have also considers multiple species models. Since much of the focus of these models is to explain the paradox of the plankton [40], they often include a variable environment which allows several species to coexist in non-equilibrium dynamics.

Ebenhoh [23] considered a linear multispecies model with n species and non-linear forcing:

$$\begin{aligned} \frac{dX_j}{dt} &= \begin{cases} (\alpha_j - \beta_j)X_j & R > R_j \\ -\beta_j X_j & R \leq R_j \end{cases} \\ \frac{dR}{dt} &= -\Sigma_{j\epsilon J(R)}\alpha_j X_j \qquad\qquad J(R) = \{j : R_j < R\} \end{aligned} \tag{1.2}$$

where X_j (numbers/volume) is the concentration of the jth algal species, $j = 1, ..., n$ each with growth rate α_j and mortality rate β_j. R_j is the growth limiting threshold for the nutrient and R is the nutrient concentration. This model also includes a nutrient pulse of amount A per unit volume at regular time intervals of length T, so that when time t is a multiple of T, the nutrient concentration is increased by A. By changing the time interval T and the nutrient pulse A, the model can allow any subset or all of the algal species to coexist.

Kishimoto [50] investigated the problem of coexistence using a nonlinear J-species model in two patches, u and w, where interpatch migration is equal in all species.

$$\begin{aligned} \frac{du_i}{dt} &= (p_i - \Sigma_{j=1}^{J} a_{ij}u_j)u_i \\ \frac{dw_i}{dt} &= (p_i - \Sigma_{j=1}^{J} b_{ij}w_j)w_i \end{aligned} \tag{1.3}$$

where $u_i(t)$ and $w_i(t)$ are the numbers of individuals of the ith species in the first and

second patches at time t, p_i are intrinsic growth rates, and a_{ij} and b_{ij} (time^{-1}numbers^{-1}) are the competition coefficients for species i and j in each patch. The assumption that the coexistence of two competitively exclusive species results in a surplus of resources implies that any number of species may coexist by taking advantage of the surplus left by the first two.

The Kierstead and Slobodkin model described in Equation 1.1 included the simple physics of diffusion. Since then, others have added more complex physical and biological dynamics to the model. Kamykowski [45] investigated the effects of semi-diurnal internal tides on phytoplankton using the theory of small amplitude waves and allowing both horizontal and vertical movement. The phytoplankton are divided into three categories, non-motile, weakly motile (do not cross variable thermocline) and motile (may cross variable thermocline). Any swimming behavior was superimposed onto the water motion. The results from simulations show that internal diurnal tides may account for patchiness observed in the field, both in abundance and in species composition. Kamykowski [46] used this model again with some modifications in order to compare the growth of a model *Gymnodium splendens* population in stationary versus wavy water columns. The wavy column model resulted in patchiness of phytoplankton populations according to environmental variations in light and water motion.

Representative of the more complex physical and biological models that have been developed, Kishi and Ikeda [49] studied a predator-prey model that includes the physical properties of wind-induced movement of sea water and a tidal current. They begin with the simple predator prey model with one phytoplankton species and one zooplankton species modelled by Michaelis-Menten uptake kinetics. This model is the basis for a two dimensional model that includes wind-induced upwelling. The results of this model show that a combination of vertical migration and upwelling are important to a red tide model.

Kishi and Ikeda also developed a three dimensional model using the Navier-Stokes

equation in the plane to generate the kinetic equations for current movements. They then constructed a compartment model which includes tidal currents in three directions, vertical migration, diffusion, and biological interactions. The authors used this model to conclude that nutrient loads and oceanographic conditions including tidal currents and wind-induced water movement influence the rapid increase in phytoplankton populations that results in a bloom.

More recently, workers have been interested in modeling the dynamics of toxic species. One such model is that of Howard et al. for cyanobacteria [38]. This aggregated model includes light- and phosphate-limited growth in a non-homogenous environment. In addition to bacterial movement, wind-induced lake mixing affects available light and nutrient concentrations. The authors were able to match existing field data suggesting that cyanobacteria populations grow most rapidly when lake conditions are calm, but continue to grow at a depressed rate during periods of lake mixing. Along the same lines is the model of Belov [9]. In this age-structured model, toxin production and release depend on cell age, nutrient availability, light, and temperature. The vertical concentration of toxin throughout the water column is modeled by a diffusion equation.

Flynn and coworkers have developed a model of toxin production for a generic toxin-producing dynoflagellate based on an aggregated model focused on the detailed physiological processes of nitrogen uptake and use by algae [26, 28, 27]. The underlying model includes uptake of ammonium and nitrate and the dynamics of the corresponding nutrient pools as affected by reduction and synthesis activities inside the cell. In order to better model toxin production, photo-acclimatization and bleaching from nitrogen deprivation were included. The driving force of toxin production is assumed to be available nitrogen either from amino acids or the protein pool. A component of the toxin may be recycled into nitrogen available for cell growth. The model produces time series data of toxin concentrations and a relationship between toxin production and light availability.

1.4 Methods - Stoichiometric Modeling

The models discussed in the previous section are intended to be a sampling of some of the characteristic models relating to algal blooms and toxic algae. We take a different approach by emphasizing individual physiology of the algae cell and focusing on biological rather than physical effects on population dynamics. Thus, we employ an individual-based algae model detailing the physiology of an algal cell with a focus on nutrient and energy flows modeled by differential equations. The individual model is incorporated into a population model using a McKendrick-von Foerster partial differential equation. The details of the model are left to Chapter 2.

The basis of the individual model is the work of Kooijman et al. [51] which makes explicit use of mass-balance conservation laws. The general approach is to track each nutrient of interest throughout the system including the processes of uptake from the external environment, assimilation into a nutrient pool, use in maintenance or growth of the organism, and breakdown from storage for reuse and excretion. A similar approach is described by Desai et al. in a model of fermentations of *Clostridium acetobutylicum* [20].

The elementary component of such a model is a transfer matrix. Consider a model with three internal components S_1, S_2, and S_3, representing protein, lipid and polysaccharides and three basic nutrients of interest, N_1 and N_2 and N_3, carbon, nitrogen and phosphorus that are taken up in the form of two external substances E_1 and E_2. Let $\nu_{i,j}$ be the number of atoms of nutrient N_i in one molecule of substance E_j. Then the uptake of nutrients into the internal nutrient pool is described by the matrix multiplication

$$\begin{bmatrix} \nu_{1,1} & \nu_{1,2} \\ \nu_{2,1} & \nu_{2,2} \\ \nu_{3,1} & \nu_{3,2} \end{bmatrix} \begin{bmatrix} \dot{E}_1 \\ \dot{E}_2 \end{bmatrix} \tag{1.4}$$

where $\dot{E}_i$ denotes the uptake rate of external substance i, which may be a function of concentration of chemical and physical parameters such as E_i and temperature. Similarly, the net gain or loss from the nutrient pool due to manufacture and breakdown of substances S_i can be summarized by the matrix multiplication

$$\begin{bmatrix} \mu_{1,1} & \mu_{1,2} & \mu_{1,3} \\ \mu_{2,1} & \mu_{2,2} & \mu_{2,3} \\ \mu_{3,1} & \mu_{3,2} & \mu_{3,3} \end{bmatrix} \begin{bmatrix} \dot{S}_1 \\ \dot{S}_2 \\ \dot{S}_3 \end{bmatrix} \tag{1.5}$$

where $\dot{S}_i$ denotes the net rate of change of substance S_i in the cell. This approach requires the assumption that all complex molecules have the same composition within type, so that, for instance, every protein is made up of the same number of carbon, nitrogen and phosphorus atoms. The above description applies to mass fluxes; however, fluxes of energy can be treated in much the same way, particularly in plant cells where the ATP molecule can be treated as the standard energy currency for the organism.

The strength of this approach is its generality. The structures, nutrients and external substances of interest can be defined to be whatever is important to the system being modelled. In addition, the stoichiometric approach to modelling ecosystems has gained speed recently. "Ecological stoichiometry" was an idea put forth by Reiners [69] in order to better explain ecosystem dynamics. While ecosystem modelers have always considered energy fluxes when constructing their models, Reiners suggests that they need to keep track of the basic elemental ratios at each trophic level in order to better describe a system, since similar organisms tend to have similar chemical composition. This is evidenced for algae by the Redfield ratio that states that carbon, nitrogen, and phosphorus are contained in algae in the ratio of 106:16:1 [68]. Using the law of conservation of matter and several axioms concerning the elemental dynamics of organisms, "theorems" including the existence of niches are deduced [69]. When stoichiometric information is included, the limiting process on an ecosystem can sometimes be delineated, while consideration of energy fluxes alone does not allow for the possibility of

nutrient limitation. At the ecosystem level, processes such as differential recycling of nutrients and life history characteristics may be explained [24]. When the stoichiometric approach with two elements, carbon and phosphorus, was applied to a classic Lotka-Volterra system, new dynamics arose including the existence of multiple equilibria, some of them exhibiting coexistence [53].

While the focus of this work is on a single species, the stoichiometric approach is still important. Since toxin production is correlated with nutrient availability and growth rate, it is logical to assume nutrients that affect toxin production should be included and tracked in the model. In addition, this approach allows for nutrient or energy limitation of individual and population growth which may give some insight into bloom dynamics as well as DA production. Finally, this model may form the basis for an ecosystem model that may include associated symbiotic bacteria and a shellfish or crustacean predator, in which case all the above arguments will apply.

1.5 Objectives

The general objective is to use the individual-based and stoichiometric modeling approaches to create and analyze a model of a toxic algae species. A system of differential equations is used to model internal cell processes and to track nutrients both in the cells and their environment. The individual model includes nutrient uptake, photosynthesis, formation of the complex cell components protein, lipid, polysaccharide, frustule, and domoic acid, and catabolism of storage in times of low energy. However, the complex nature of chemical processes such as the Krebs' cycle and specific biochemical details of frustule formation are not included.

The wealth of experimental data on the species *Pseudo-nitzschia multiseries* allows us to validate the model by fitting it to experimental data. In particular, Pan and coworkers performed a set of experiments in batch and chemostat cultures during which they tracked population density, toxin levels in the cells and medium, and silicate

concentration in the medium [58, 59]. A valid model was defined as one that resulted in outputs within 25% of experimental population numbers and evidenced the high levels of toxin production attained at the end of batch culture experiments. In the batch culture, a population was introduced into a nutrient-containing medium and allowed to grow undisturbed until nutrients became depleted and growth stopped. The model will be used to represent the data associated with batch culture, emphasizing population dynamics, high levels of domoic acid concentrations occurring during stationary phase, and a qualitative fit to external silicate. A sensitivity analysis is also done in this setting to determine governing parameters and any interactions between them.

The experiments in the chemostat are particularly important to validating the model. Since the chemostat system allows constant flow through the system, it more closely resembles the dynamics that may occur in an ocean environment. Therefore, it is important that the model can mimic these experiments in addition to those in batch. The experiments performed on chemostat cultures showed much higher toxin levels than those in the batch culture possibly due to the use of a different strain of the algae. Comparing the parameter values required to fit batch and chemostat experiments may give some insight into the physiological differences between the two strains.

An investigation of model behavior under varying environmental conditions in the chemostat will also be performed. This may help to characterize nutrient regimes that cause different levels of toxin production and uncover strengths and weaknesses in the model. In addition, some recommendations for further biological experimentation may be made based on the results of this investigation.

Chapter 2

The Individual-Based Population Model for the Diatom *Pseudo-nitzschia multiseries*

The model discussed here forms the basis of this work. It is an extension of the model developed by Hurlebaus [39] and Miller [55] to model a generic algae species (Figure A.3). The state variables for the system are mass of protein, m_{Pr} (μmol), mass of lipid, m_{Lp} (μmol), and mass of polysaccharide, m_{Ps} (μmol). The mass of frustule, m_{Fr} (μmol), is included as well but is not a state variable since it changes only in relation to reproduction. (All model variables are listed in Table B.2 and parameters are listed in Table B.3.) Each algae cell takes up external substances from the environment and deposits them into the nutrient pools. Photosynthesis builds the energy pool which is used for maintenance and growth. The pools are depleted through anabolism to create proteins, lipids, polysaccharides, frustule, or domoic acid and can be replenished through catabolism of polysaccharides, lipids and proteins in times of nutrient or energy limitation. Modifications have been made to the individual model to describe silicon uptake kinetics, formation of a frustule, and production of domoic acid. At the population level, life cycle peculiarities of diatoms including shrinking during cell division and sexual reproduction have been added.

2.1 The Individual Model

2.1.1 Uptake Kinetics

The external nutrients modeled are nitrogen (N) in the forms of nitrate (NO_3^-) and ammonium (NH_4^+); phosphorus (P) as orthophosphates and other phosphates; iron (Fe); and silicon (Si), in the form of silicic acid (SiO_2). Carbon (C) is considered to be plentiful in the environment and is treated separately in relation to photosynthesis. With the exception of silicic acid and carbon, the uptake rate, $\rho_{up,\phi}$, for external nutrients (ϕ) is based on Michaelis-Menten kinetics multiplied by an internal inhibitory term that provides for saturation of nutrient. This prevents internal nutrient pools from increasing indefinitely.

$$\rho_{up,\phi}(\phi_e, T, \phi_i) = \begin{cases} \left(\frac{1}{\frac{a}{v(T)} + \frac{c_{\phi_e}}{\phi_e}}\right)\left(1 - \frac{\phi_i}{c_{\phi_i} m_{Pr} + \phi_i}\right) n_{\phi_e} SA & \phi_e > 0 \\ 0 & \phi_e = 0 \end{cases} \tag{2.1}$$

where ϕ_e (μmol cm^{-3}) and ϕ_i (μmol) are the external and internal concentrations of nutrient ϕ respectively, T is water temperature, a (cm) is the cell wall thickness, c_{ϕ_e} (s cm^{-3}) is a proportionality constant associated with nutrient ϕ, c_{ϕ_i} (nd) is a constant reflecting the effect of the internal concentration of nutrient (ϕ_i) on uptake rate, m_{Pr} is the mass of protein in the cell, n_{ϕ_e} (cm^{-2}) is the density of transport sites for uptake of nutrient ϕ on the cell surface and SA (cm^2) is the cell surface area. The transport velocity $v(T)$ is given by the Arrhenius equation

$$v(T) = Se^{\left(\frac{T_A}{T_1 T}(T - T_1)\right)} \tag{2.2}$$

where S (μmols cm s^{-1}) is a rate constant, T_A (degrees Kelvin) is the Arrhenius temperature and T_1 (degrees Kelvin) is the chosen reference temperature at which the velocity equals the rate constant.

The surface area of the cell is assumed to be directly related to volume which is a function of mass of protein $m_{Pr,0}$, mass of lipid, $m_{Lp,0}$, and mass of polysaccharide

$m_{Ps,0}$ of the cell immediately following cell division or when a new cell is created through sexual reproduction.

$$SA = V^{2/3} = \left(\frac{m_{Pr,0}}{\sigma_{Pr}} + \frac{m_{Lp,0}}{\sigma_{Lp}} + \frac{m_{Ps,0}}{\sigma_{Ps}} \right)^{2/3} \tag{2.3}$$

where σ_{Pr} (μmols cm^{-3}), σ_{Lp} (μmols cm^{-3}), and σ_{Ps} (μmols cm^{-3}) are the molecular densities of protein, lipid, and polysaccharide, respectively.

The expression for silicon uptake is similar to the uptake of other nutrients. However, silicic acid uptake by diatoms has been shown to be a carrier-mediated process [71] which may be less effective at low concentrations than at higher ones. Therefore, the Michaelis-Menten part of the expression is modified by making it dependent on the square of the external concentration giving it the general form of a type III functional response,

$$F(x) = \frac{Mx^2}{k + x^2} \tag{2.4}$$

While adding the square changes the uptake rate and the half saturation constant to $\sqrt{k}$, the saturation level remains the same. Also, the classic form is concave down for positive x, but this function is concave up when $x > 0$ but close to 0, and changes concavity at $\sqrt{\frac{k}{3}}$ (Figure A.4). Thus this representation assumes that for small concentrations the uptake sites may not be exposed to silicon, but increases in concentration result in higher increases in uptake rate until there are few unused transport sites left and then the uptake rate increases less with increased concentration. Another difference in the uptake function for silicon is that the inhibition term is the ratio of the mass of silicon in the pool and frustule with a multiple of the mass of frustule immediately preceding cell division $2m_{Fr_0}$. No uptake of silicon occurs if the total silicon in the pool and frustule is greater than a constant, c_{Fr} times the amount of silicon needed to lay down the hypothecae of the daughter cells. Finally, because diatoms have been shown to adapt to low nutrient concentrations by increasing their ability to take up that nutrient [18, 44],

the entire expression for silicon uptake is multiplied by a decaying exponential function that affects uptake only at low external silicon concentrations. Therefore, the uptake rate of silicon, $\rho_{up,Si}$, is given by

$$\rho_{up,Si}(Si_e, T, Si_i) = \begin{cases} L(Si_e)\left(\frac{1}{\frac{a}{v(T)}+\frac{c_{Si_e}}{Si_e^2}}\right)\left(1-\frac{Si_i+m_{fr}}{2c_{Si_i}m_{Fr_0}}\right)n_{Si_e}SA & Si_i + m_{Fr} < c_{Fr}m_{Fr_0} \\ & \text{and} \quad Si_e > 0 \\ 0 & \text{otherwise} \end{cases} \tag{2.5}$$

where

$$L(Si_e) = 1 + \lambda_0 e^{-\rho Si_e}. \tag{2.6}$$

Si_e (μmol cm^{-3}) and Si_i (μmol cm^{-3}) are external and internal silicon concentrations, c_{Si_e} (s cm^{-3}) is the proportionality constant associated with external silicon, c_{Si_i} (nd) reflects the effect of the internal concentration of silicon on uptake rate, c_{Fr} (nd) is a constant, and n_{Si_e} (cm $^{-2}$) is the density of transport sites for silicon per cell surface area. The constant c_{Fr} multiplies the initial amount of silicon in the cell; when the total amount of silicon in the frustule and nutrient pool reaches this multiple of the initial amount, silicon uptake ceases. $L(Si_e)$ can be interpreted as a measure of the efficiency of silicon uptake, which increases at very low silicon concentrations. Therefore, the constant λ_0 (nd) is the maximum additional uptake efficiency and ρ measures the rate of efficiency loss per unit of external silicon concentration. The addition of the $L(Si_e)$ multiplier changes the shape of the uptake curve by providing a local maximum at low silicon concentrations (Figure A.5).

2.1.2 Photosynthesis and Carbon Uptake

Photosynthesis, one of the most important processes of an algae cell, provides the cell with the energy (ATP) and the carbon needed to build protein and storage components and to carry on other energy requiring cell processes. After conducting exper-

iments with *Pseudo-nitzschia multiseries*, Pan [62] concluded that the photosynthesis-irradiance curve proposed by Platt et al. [65] was the best fit for the species. This curve was developed to address the problem of photoinhibition with a continuous rather than a piecewise continuous function. The assumption is that photosynthesis is linearly related to irradiance when it is low, and slowly saturates at higher irradiances. Photoinhibition was added as a process independent of the original model parameters (P_{max}, α).

The relationship between photosynthetic rate and irradiance is given by

$$P(I) = P_{max}(1 - e^{-\alpha I/P_{max}})e^{-\beta I/P_{max}} \tag{2.7}$$

where P_{max} (μmolC[μmolCbiomass]$^{-1}s^{-1}$) is the maximum photosynthetic rate in the absence of photoinhibition, α (μmolC[μmolCbiomass]$^{-1}s^{-1}$[μmolm^{-2}s^{-1}]$^{-1}$) is the initial slope of the photosynthesis irradiance curve. I ([μmolm^{-2}s^{-1}]$^{-1}$) is irradiance, and β (μmolC[μmolCbiomass]$^{-1}s^{-1}$[μmolm^{-2}s^{-1}]$^{-1}$) is the photoinhibition index.

Carbon, adsorbed as CO_2, is assumed to be plentiful in the environment. Therefore, the uptake rate depends only on photosynthetic rate and surface area of the cell according to the following equation:

$$\rho_{up,C}(I) = P \times SA \tag{2.8}$$

The basic unit of energy in the model is adenosine triphosphate (ATP), denoted E (μmols). The cell gets energy either from photosynthesis or catabolism. The model sets the amount of ATP produced through photosynthesis at twice the amount of carbon taken up, representing the process of non-cyclic photophosphorylation. It should be noted that there may be by-products produced by this process that can generate additional ATP, but this is not included in the model [66].

2.1.3 Structure and Storage

Once nutrients have been incorporated into internal pools and ATP has been produced from photosynthesis, those elements are used to create proteins, frustule, polysaccharides and lipids. A functional response associated with the building of each of these substances is constructed that takes into account all the necessary nutrients and ATP required to make one molecule of the cell. The creation of one molecule of any substance is a function of the internal concentrations of its components. The functional response takes into account a wait time associated with the arrival of each constituent from the nutrient pool to a location where the substance will be constructed. Therefore to provide a common currency for the model, the rate of production is proportional to the most limiting nutrient, i.e. the one with the highest waiting time associated with it. Each functional response is normalized to one atom of carbon except that of the frustule, which is normalized to one atom of silicon.

The functional responses for proteins, frustule, polysaccharides and lipids are as follows:

$$f_{Pr}(E,C_i,N_i,P_i) = \begin{cases} \frac{1}{\max(\frac{k_{C,Pr}C_{C_i}}{C_i},k_{N,Pr}\frac{C_{N_i}}{N_i},k_{P,Pr}\frac{C_{P_i}}{P_i},k_{E,Pr}\frac{C_{E_i}}{E})+\frac{1}{I_{m,Pr}}} & C_i,N_i,P_i,E>0, \\ 0 & \text{otherwise;} \end{cases} \tag{2.9}$$

$$f_{Fr}(E,Si_i) = \begin{cases} \frac{1}{\max(\frac{k_{Si,Fr}C_{Si_i}}{Si_i},k_{E,Fr}\frac{C_{E_i}}{E})+\frac{1}{I_{m,Fr}}} & Si_i,E>0, \\ 0 & \text{otherwise;} \end{cases} \tag{2.10}$$

$$f_{Ps}(E,C_i) = \begin{cases} \frac{1}{\max(\frac{k_{C,Ps}C_{C_i}}{C_i},k_{E,Ps}\frac{C_{E_i}}{E})+\frac{1}{I_{m,Ps}}} & C_i,E>0, \\ 0 & \text{otherwise;} \end{cases} \tag{2.11}$$

$$f_{Lp}(E,C_i,P_i) = \begin{cases} \frac{1}{\max(k_{C,Lp}\frac{C_{C_i}}{C_i},k_{P,Lp}\frac{C_{P_i}}{P_i},k_{E,Lp}\frac{C_{E_i}}{E})+\frac{1}{I_{m,Lp}}} & C_i,P_i,E>0, \\ 0 & \text{otherwise;} \end{cases} \tag{2.12}$$

where ϕ_i (μmol) is the internal mass of substance ϕ, C_{ϕ_i} (s) is the wait time for a

molecule of substance ϕ, k_{ϕ_i,ϕ_s} (μmol/s) relates the number of atoms of substance ϕ_i used to make ϕ_s per unit C per unit time, and I_{m,ϕ_s} (nd) represents the building time for one molecule of substance ϕ_s.

The two storage components, polysaccharide and lipid, can be processed via catabolism in times of low energy to release energy and nutrients back into the pools. The catabolic rates, g_{Ps} (μmols s^{-1}) and g_{Lp} (μmols s^{-1}) are inversely proportional to the amount of ATP in the energy pool and are given by

$$g_{Ps} = k_{Ps,0}\left(1 + \frac{k_{Ps,3}}{P_i}\right)\frac{1}{k_{Ps,1} + k_{Ps,2}\frac{E}{m_{Ps}}}, \tag{2.13}$$

$$g_{Lp} = k_{Lp,0}\left(1 + \frac{k_{Lp,3}}{P_i}\right)\frac{1}{k_{Lp,1} + k_{Lp,2}\frac{E}{m_{Lp}}}, \tag{2.14}$$

where $k_{\phi_s,0}$ (μmols s^{-1}) is the maximum catabolic rate of substance ϕ_s, $k_{\phi_s,1}$ and $k_{\phi_s,2}$ (nd) and $k_{\phi_s,3}$ (μmols) are constants.

Combining the functional responses with catabolism gives differential equations for each of the four components.

$$\frac{dm_{Pr}}{dt} = m_{0,Pr}f_{Pr}(E, C_i, N_i, P_i), \tag{2.15}$$

$$\frac{dm_{Fr}}{dt} = m_{0,Fr}f_{Fr}(E, Si_i), \tag{2.16}$$

$$\frac{dm_{Lp}}{dt} = m_{0,Lp}f_{Lp}(E, C_i, P_i) - g_{Lp}, \tag{2.17}$$

$$\frac{dm_{Ps}}{dt} = m_{0,Ps}f_{Ps}(E, C_i) - g_{Ps}, \tag{2.18}$$

where m_{0,ϕ_s} (μmol s^{-1}) is the maximum number of ϕ_s molecules fixed per unit time.

2.1.4 Domoic Acid Production

The biochemical pathway leading to domoic acid production is still not completely known. In the model, the production of domoic acid is treated much like the production of the cell components protein, lipid, polysaccharide and frustule. However, there are two differences. Domoic acid is produced after all structure and storage components

so that synthesis occurs only if there is excess energy and nitrogen available in the pools. This is a reasonable assumption since very little domoic acid is produced when cultures are actively dividing in the exponential growth phase and production increases as the population growth rate slows down [58]. In addition, since DA production has been shown to increase with decreased external silicon, we make the assumption that the maximum rate of DA production is related to the changes in physiology required to increase silicon uptake during times of low external silicon concentration. Thus, a formulation for domoic acid production that satisfies these assumptions is

$$\frac{dm_{DA}}{dt} = m_{0,DA} L(Si_e) f_{DA}(E, C_i, N_i), \tag{2.19}$$

where $m_{0,DA}$ is the maximum number of domoic acid molecules fixed per unit time, $L(Si_e)$ is given in Equation 2.6. The functional response f_{DA} is given by

$$f_{DA}(E, C_i, N_i) = \frac{1}{\max(\frac{C_{C_i}}{C_i}, k_{N,DA}\frac{C_{N_i}}{N_i}, k_{E,DA}\frac{C_{E_i}}{E}) + \frac{1}{I_{m,DA}}} \tag{2.20}$$

where $k_{N,DA}$ (μmol) and $k_{E,DA}$ (μmol) are the number of nitrogen and ATP molecules needed to create one molecule of domoic acid, respectively and $I_{m,DA}$ (nd) is the maximum reaction rate for one molecule of DA.

2.1.5 Energy Dynamics

In addition to the energy required to create cell structures, domoic acid and the energy gained from photosynthesis, there are two other components that affect the change in energy in a cell. We take into account the energy needed to maintain the cell and the energy that can be gained through respiration. Cell maintenance is assumed to be directly proportional to the total internal (non-frustule) mass:

$$M = M_0(m_{Ps} + m_{Lp} + m_{Pr}) \tag{2.21}$$

where M_0 ($s^{-1}\mu mol^{-1}$) is the maintenance cost associated per unit biomass. Respiration is given as a fraction of available carbon

$$R(C_i) = j_C C_i \tag{2.22}$$

where j_C (s^{-1}) is the fraction of the carbon pool respired per second.

Combining all the energy supply processes and energy demand processes, we get the change in the energy pool per unit time:

$$\frac{dE_i}{dt} = \mu_{ATP,CO} P(I) - k_{E,Pr}\frac{dm_{Pr}}{dt} - k_{E,Lp}\frac{dm_{Lp}}{dt} - k_{E,Ps}\frac{dm_{Ps}}{dt} - k_{E,Fr}\frac{dm_{Fr}}{dt} - k_{E,DA}\frac{dm_{DA}}{dt} - M + \mu_{ATP,CO} R. \tag{2.23}$$

Recall that $P(I)$ is the photosynthetic rate, M is the maintenance rate and R is the respiration rate. The constant $\mu_{ATP,CO}$ (μmol) is the number of moles of ATP produced when a mole of CO_2 is used in the Krebs cycle.

2.1.6 Nutrient Pool Dynamics

Similarly to the energy flux, nutrient pool fluxes are simply the summation of all nutrient-providing and nutrient-requiring processes. Therefore, the equations below represent the transition matrices discussed in Section 1.4.

The carbon flux is dependent on photosynthesis, respiration, domoic acid, and anabolism and catabolism of protein, lipid, and polysaccharides:

$$\frac{dC_i}{dt} = P + \frac{dm_{Pr}}{dt} + \frac{dm_{Lp}}{dt} + \frac{dm_{Ps}}{dt} + \frac{dm_{DA}}{dt} - R. \tag{2.24}$$

Note that constants relating carbon to each component are not necessary since the parameters have been normalized to one carbon atom.

The nitrogen flux is dependent on uptake, anabolism of proteins, and domoic acid production:

$$\frac{dN_i}{dt} = \rho_{up,NO_3} + k_{N,Pr}\frac{dm_{Pr}}{dt} + k_{N,DA}\frac{dm_{DA}}{dt}. \tag{2.25}$$

$k_{N,Pr}$ and $k_{N,DA}$ are the number of nitrogen atoms needed to create one molecule of protein and one molecule of domoic acid, respectively.

Phosphorus flux is dependent on uptake of orthophosphates and other phosphates, protein and lipid flux. In addition, three phosphorus atoms are used or released whenever a molecule of ATP is created or used, respectively:

$$\frac{dP_i}{dt} = \rho_{up,OP} + \rho_{up,OR} + k_{P,Pr}\frac{dm_{Pr}}{dt} + k_{P,Lp}\frac{dm_{Lp}}{dt} - 3\frac{dE_i}{dt}. \tag{2.26}$$

$k_{P,Pr}$ and $k_{P,Lp}$ are the number of nitrogen atoms needed to create one molecule of protein and one molecule of lipid, respectively.

Finally, silicon flux is given by silicic acid uptake and frustule dynamics:

$$\frac{dS_i}{dt} = \rho_{up,SiO_2} + \frac{dm_{Fr}}{dt}. \tag{2.27}$$

2.1.7 External Factors

The equations governing the external concentrations of nutrient are simple mass-balance equations:

$$\frac{d\phi_e}{dt} = \rho_{in,\phi_e} - \sum_{species}\sum_{ecotypes} \rho_{up,\phi}\delta_{sp,e} \tag{2.28}$$

where ρ_{in,ϕ_e} (μmol $\mathrm{l}^{-1}\mathrm{s}^{-1}$) is the input of substance ϕ into the ambient water and $\delta_{s,e}$ (cells l^{-1}) is the density of cells of ecotype e and species sp.

2.2 The Population Model

The individual model is incorporated into a population model which tracks individuals grouped by mass of protein, mass of lipid, and mass of polysaccharide. The classic McKendrick-von Foerster partial differential equation model is

$$\frac{\partial\delta}{\partial t} = \sum_{i=1}^{3}\frac{\partial}{\partial m_i}(\phi_i(m)\delta) - D\delta \tag{2.29}$$

where δ (cells/liter) is the population density, $m = (m_{Pr}, m_{Lp}, m_{Ps})$ is the vector of state variables, $\phi_i(m)$ is the derivative with respect to time of m_i, and D (s^{-1}) is the death rate. This equation requires a boundary condition representing new cell production

$$B(t) = \int_0^\infty \int_0^\infty \delta(t, m_{Ps}, m_{Lp}, 2m_{Pr,0}) + \int_0^\infty \int_0^\infty \delta(t, m_{Ps}(1-l), m_{Lp}(1-l), 2m_{Pr,0}(1-l)) dm_{Lp} dm_{Ps} + \int_0^{m_{Pr,Tr}} \frac{1}{2}\delta(t, m_{Ps}, m_{Lp}, m_{Pr}) dm_{Pr} \quad (2.30)$$

The first and second terms represent individuals which are the result of cell division where $m_{Pr,0}$ is the initial protein level of the cell, and l represents the loss of biomass when the smaller cell is produced. The third term represents individuals resulting from sexual reproduction, where $m_{Pr,Tr}$ is the mass of protein that triggers the cell to produce gametes. We assume only one auxospore is produced per sexually reproducing pair.

2.2.1 Mortality

Mortality of the cells occurs either through sinking or grazing. Sinking is a function of cell volume V (cm^3) and depth of the surface layer z (m):

$$\frac{x}{z}\delta(t, V) \quad (2.31)$$

where V is calculated from equation 2.3 and is a function of m_{Ps}, m_{Lp}, and m_{Pr}. The grazer is modeled by an aggregated model using Michaelis-Menten dynamics, where grazing rate depends on the volume of the algae cells:

$$\frac{dZ}{dt} = M_i A_e \frac{\Sigma_{species}\Sigma_{ecotypes}\Sigma_{cohorts} q(x)\delta(t, V)}{\Sigma_{species}\Sigma_{ecotypes}\Sigma_{cohorts} q(x)\delta(t, V) + \kappa} Z - \theta Z \quad (2.32)$$

where Z ($\#/m^3$) is grazer density, M_i is the maximum ingestion rate of the grazer, A_e represents its assimilation efficiency, $q(x)$ is the probability a grazer will ingest a cell with volume V, κ is the half saturation constant and θ represents a constant rate of mortality. From the above expression, the losses from each algae cohort will be $q(x)\delta(x, t)$.

2.3 Model Implementation

The model is implemented through a computer code written in the C programming language and compiled with `gcc`. A thirty-day simulation with a single cohort takes 39 CPU seconds when the program is run on a PC with a Pentium III 800 MHz processor running Linux 8. A two-step Runge-Kutta method with step size of two seconds is used to solve the differential equations in the individual model. While in nature, cell processes would be occurring simultaneously, writing a computer code requires that processes be prioritized. For example, the anabolic processes for protein, lipid and polysaccharide all require energy; if we allow them to proceed based on the same available energy in the energy pool, this may result in an overdraw and a negative value for the energy pool. To avoid this problem, the processes are prioritized so that each subsequent process proceeds according to what is left from the previous ones (Figure A.7).

Logically, the first task the cell performs is to set aside the necessary energy for maintenance since without this, the cell could not survive. It then begins to take up nutrients from the enviroment and places them into the nutrient pools where they become immediately available for the subsequent processes in the same time step. Uptake is followed by photosythesis. Therefore, the pools become replenished before any of the other model processes continue.

We assume the cell puts resources into growth before storage, therefore the anabolic processes are ordered so that protein is created first, followed by lipid, polysaccharide and frustule. Frustule is given last priority because the cell likely creates frustule only after the protoplasm is ready to divide [72]. While the model does not exactly mimic the natural behavior, as frustule is constantly incorporated, making frustule formation follow production of all other structure and storage components is a good approximation. Finally, if there are nutrients and energy left in the pools, the cell pro-

duces DA, possibly as a secondary metabolite. Anabolism is followed by catabolism of polysaccharide and lipid in that order.

Another important component to the model implementation is that some of the cell processes cease when cell protein has doubled but the cell division has not yet been completed due to a lack of silicon. Once protein has doubled, the cell does not absorb any nutrients except silicon. In addition, anabolism of protein, lipid, and polysaccharide and catabolism no longer occur. Instead, the cell puts all of its resources into building the hypothecae of the daughter cells and may also produce DA if there is extra energy and nutrients in the pools to do so. During this phase, maintenance costs continue to contribute to losses from the energy pool while photosynthesis continues at a reduced level.

Chapter 3

Model Validation and Sensitivity Analysis

A series of batch culture experiments was performed by Pan and coworkers to investigate the effects of silicate limitation on the dynamics and domoic acid production of a population of *Pseudo-nitzschia multiseries* [58]. The first of the three experiments served as the basis for a sensitivity analysis in order to determine the parameters that most affect population, total domoic acid, and external silicon dynamics. Subsequently, model output for these three variables was compared to the experimental data in the paper. All the results of this chapter were obtained by setting the parameter λ_0 in Equation 2.5 equal to zero. The initial structure of the model population included 10 cohorts distributed uniformly over the range of mass of protein and mass of frustule of an individual diatom cell, representing cells in varying stages of growth. Thus, $L(Si_e) = 1$, the Si uptake rate is modelled by the modified Michaelis-Menten curve in Equation 2.5 and domoic acid production follows the exact same functional response as protein, lipid, polysaccharide and frustule.

The following sensitivity analysis will show that the parameters that resulted in the most dramatic changes in model output could be grouped into three categories: photosynthesis, energy dynamics, and silicon dynamics. For photosynthesis, the significant parameters were α, β, and P_{max} (Equation 2.7), while C_E (Equations 2.9, 2.10, 2.11, 2.12) and $k_{E,Pr}$ (Equation 2.9) were the sensitive parameters related to internal energy dynamics. Finally, the parameters T_1 (Equation 2.2) and n_{Si} (Equation 2.5) affecting

Si uptake and C_{Si} and $M_{0,Fr}$ (Equation 2.10) affecting frustule dynamics also showed sensitivity. These results are not surprising since cell growth and reproduction require energy and nutrients and the experiments were set up such that Si was the limiting nutrient.

Overall the model output was qualitatively close to the data. The model was best at predicting population dynamics where the average relative error between the model and the data was at most 25% for each of the three experiments. The DA dynamics were harder to capture, as it was difficult to fit both the low inital levels of DA and the high final levels simultaneously for all three experiments. For external silicon, the model output was closest to the data for experiments A and C, but did not fare as well in experiment B.

3.1 Biological Data

In a batch experiment, a culture is introduced to a nutrient-containing medium and allowed to grow undisturbed. Measurements are taken periodically to determine the levels of biomass and nutrients in the system. In the paper, three separate experiments were performed simultaneously on populations derived from the same algae strain. Experiment A had an initial Si concentration of 95.3 μmol/l while experiment B had initial Si concentration 190.5 μmol/l. Experiment C began with 60.9 μmol/l Si, was allowed to grow undisturbed for 14 days, after which 64 μmol Si was added. Cell concentration, external Si concentration, chlorophyll a concentration, and domoic acid levels were measured.

The data for these experiments (Figures A.8 , A.9 and A.10) show some interesting dynamics, particularly for DA and external Si. The authors state that DA production occurs in two phases. The first phase occurs as the population growth rate begins to decline and is characterized by low DA production. The second phase shows higher DA production and occurs when population growth has almost stopped. The onset of the

second phase occurs near day 30 in experiment A and day 25 in experiment B. Due to the addition of Si to the medium in experiment C, the second phase is not reached. The cells do not appear to switch instantaneously from the first to the second phase, rather there appears to be a five to ten day adjustment period of slightly increased production which we will refer to as the *transition phase*. In addition, there were a few data points which reflected a decrease in the total domoic acid levels in experiments A and C. Since DA is a stable compound, it is strange that the total amount in cells and medium would decrease. No explanation for these points is offered by the authors.

The data for external silicon concentration imply that cells are able to excrete silicon into the medium. In both experiments A and C, the data fluctuate from decreasing to increasing, while in experiment B, external Si decreases for the first 15 days and gradually increases for the remaining 30 days. It should be noted that for experiment B, the error bars for external silicon imply that this constant increase may not be an accurate representation of the dynamics.

3.2 Sensitivity Analysis

A sensitivity analysis was performed using the external conditions of Experiment A above as the initial external conditions for the model. Before beginning the sensitivity analysis, we obtained a parameter set that resulted in model output within 25% of the population data for experiment A while capturing the high level of DA at the end of the experiment. This was accomplished by using the original parameter set from Miller [55] and changing any parameter values that could be obtained from other sources (Table B.4). This parameter set was further varied to satisfy the criteria mentioned and the model was allowed to run for 40 days. The output from this parameter set was used as the basis for the sensitivity analysis. Population level, external Si concentration, and total DA in the cells and medium was written every 24 minutes resulting in 2400 data points per variable. The variation from the base was measured by the mean relative

error:

$$\frac{1}{2400}\sum_{n=1}^{n=2400}\frac{|D_{b,n}-D_{p,n}|}{D_{b,n}} \tag{3.1}$$

where $D_{b,n}$ is the nth value of the base simulation and $D_{p,n}$ is the nth value of the perturbed simulation.

The first set of perturbation experiments was used to determine the parameters which resulted in the most deviation in population, total DA, and external Si dynamics. Each of the 62 parameters was varied by ten and fifty percent above and below the base value for a total 248 simulations. There were five parameters with a mean absolute deviation in population size and total DA greater than ten percent when perturbed ten percent: the wait time associated with energy, C_E, the photoinhibition index β, the maximum photosynthetic rate, P_{max}, the reference temperature, T_1, and the number of ATP molecules required to produce a protein molecule, $k_{E,Pr}$. The same parameters along with the maximum number of frustule molecules fixed per time, $M_{0,Fr}$, resulted in a deviation greater than fifty percent when perturbed fifty percent. Additionally, at the ten percent level, all the response variables (population, DA, external Si) were sensitive to four parameters with a deviation of at least one percent. These were the initial slope of the photosynthesis irradiance curve (α), the Si wait time (C_{Si_i}), the number of transport sites for Si uptake per unit area (n_{Si}), and $M_{0,Fr}$.

Based on these results, a full factorial design varying the five parameters C_{E_i}, β, P_{max}, T_1, and $k_{E,Pr}$ by plus and minus twenty percent and plus and minus ten percent was done to determine which parameters were contributing most to the deviation and whether there were any important interactions between them. For population size, total DA, and external Si, the mean absolute error was calculated. These data sets were analyzed using two way ANOVA with constrained sum of squares.

The population data showed that C_E was overwhelmingly responsible for the variability in the data (F = 4333.22, p = 0) (Table B.5). Recall that the p-value is the

probability that the means of the two samples would differ as they did given that they were actually the same so that a very small p-value implies that there is almost definitely a difference in the two means. In most of the simulations where C_E was reduced by twenty percent and several at the ten percent reduction the algae population became extinct before the end of the simulation, accounting for the disproportionately large amount of the variability attributed to C_E. In order to determine whether there were other factors influencing population data, several more ANOVA tests were performed. The first was done omitting C_E and showed that the other factors influencing population are T_1 (F = 43.47, p = 0), P_{max}, (F = 12.4, p = 0) and the interaction between T_1 and $K_{E,Pr}$ (F = 2.02, p = 0.0096). Secondly, if the simulations that resulted in extinction were removed from the data set, then T_1 (F = 2998.65, p = 0), C_E (F = 352.44, p = 0), and P_{max} (F = 102.1, p = 0) were most influential. Finally, all the simulations where C_E was reduced by twenty percent were removed from the data set, showing similar results as the original ANOVA (Table B.6). It is not surprising that two of the three parameters that strongly affected population dynamics, C_E and P_{max}, were related to the cell energy dynamics, since energy is required for all cell processes involving growth and reproduction. The other important parameter, T_1, appears because it helps to determine the rate of nutrient uptake for the cells, which is related to how fast cell structures can be built.

For domoic acid, the results were simpler since C_E did not overwhelm the data (Table B.7). The most important single factors were T_1 (F= 625.6, p = 0), $K_{E,Pr}$ (F = 202.32, p = 0), and C_E (F = 162.49, p = 0). The most important interaction excluding interactions between the three parameters mentioned was P_{max} with T_1 (F = 65.75, p = 0). While it is clear that T_1 and C_E can be important to DA production because the amount of nutrients available to make it depends on the uptake rate and available energy, it is not so obvious that DA production should be particularly sensitive to $K_{E,Pr}$. However, recall that domoic acid is produced only after anabolism has been performed,

therefore, the amount of energy used to create protein affects the amount of energy that will be left for domoic acid production. In addition, the rate of protein production determines the time spent between protoplasm division and cell division when the cell has an opportunity to produce large amounts of DA.

The Si data is closely tied to the population data since the population size has a direct affect on the total amount of Si is taken up from the medium. Therefore, the statistical analysis of the sensitive parameters was similar to that of the population data. Since C_E overwhelmed the results, the same approach was taken with these data as with the population data, removing various subsets from the data set to determine if any other parameters might be driving the system. Again, C_E (F = 4296.38, p = 0) and T_1 (F = 3576.2, p = 0) were the most important parameters when the analysis was done on the whole data set. However, in these data, the amount of variability was more evenly shared by these two parameters. When C_E was not considered, P_{max} (F = 15.37, p = 0) was somewhat important second to T_1 (F = 420.44, p = 0) and the only significant interaction was between T_1 and $K_{E,Pr}$ (F = 2.83, p = 0.0001). These results are very similar to those obtained for the population data. When the simulations in which the algae population did not survive were removed from the data set, T_1 (F = 85051.67, p = 0), $K_{E,Pr}$ (F = 120.18, p = 0) and C_E (F= 93.08, p = 0) accounted for most of the variability. This is a difference between these data and the population data. In the population data for this experiment, $K_{E,Pr}$ is the least important single variable. While the energy required for protein does not determine when the cell divides, it does help determine the rate at which the cell reaches the stage where protoplasm has divided, and therefore determines when Si will begin to be quickly incorporated into the frustule. If this happens earlier, less total Si will be taken up by the cell because it will not have time to accumulate a large amount in the pool while more will be taken up if this happens later. The experiment omitting simulations with a twenty percent decrease in C_E showed the same parameters that were important to population dynamics, T_1 (F

= 3020.52, p = 0) and C_E (F = 966.8, p = 0), were important to external Si dynamics. However, T_1 had more effect on Si than C_E since T_1 is directly related to uptake rate.

A second factorial experiment was performed using the same parameters as in the five factorial experiment with the addition of $M_{0,Fr}$, C_{Si_i}, and n_{Si}. These three parameters were chosen because together with α, they showed at least a one percent deviation in all the response variables. The parameter α was not included in the factorial experiment because the parameters P_{max} and β were already included. Since irradiance was kept constant, the inclusion of α would not give additional information.

The population data showed three parameters contributing most to the variability in the data, C_E (F = 3068.84, p = 0), $M_{0,Fr}$ (F = 2156.16, p = 0) and T_1 (F = 673.88, p = 0) (Table B.10). Population dynamics are very sensitive to $M_{0,Fr}$ since the biological experiment was constructed so that Si would drive the system and this parameter determines the rate at which the cells can incorporate Si into frustules(Equation 2.10). When the simulations in which the population went to extinction were omitted, T_1 (F = 18495.63, p = 0) was the factor that was most responsible for the variability in the population data, with $M_{0,Fr}$ (F = 554.97, p = 0) and C_{Si_i} (F = 522.27, p = 0) also contributing. Because C_{Si_i}, the internal wait time for Si, helps determine the rate of frustule formation (Equation 2.10), it makes sense that this parameter was important to population dynamics along with $M_{0,Fr}$. The only interaction not including C_E, T_1, and $M_{0,Fr}$ which had any importance was P_{max} with β (F = 347.36, p = 0 for simulations excluding extinction), however, this is because both of these parameters appear in the photosynthesis- irradiance curve (Equation 2.7)

For domoic acid, the addition of three parameters to the original experiment did not provide new information, implying that the process of DA production was not sensitive to the parameters related to Si uptake (Table B.12). In the experimental data, however, there is a clear correlation between Si concentration and DA production. Therefore, we may conjecture that the correlation of these two quantities may not be

directly linked, but may be due to other factors. For example, when the protoplasm has divided but the new frustules are still being formed, there may be extra energy or nitrogen available which can not be used for growth during that part of the cell cycle.

The external Si data for the eight parameter factorial experiment seemed to follow the population data as was the case in the five parameter experiment. Again C_E (F = 3316.4 p = 0), $M_{0,Fr}$ (F = 1774.26, p = 0) and P_{max} (F = 375.8, p = 0) were the most sensitive parameters (Table B.13). When the simulations resulting in extinction were removed from the data set, T_1 (F = 7089.18, p = 0) had the most effect on external Si while P_{max} (F = 600.52, p = 0) continued to be very influential (Table B.14). It may seem counterintuitive that external Si dynamics are more sensitive to P_{max} than population dynamics are. This can be explained by the fact that in the biological experiment, the culture was set up so that Si would force the population dynamics. Therefore, while energy is not as strong a factor in the rate of population growth, it strongly affects Si uptake. The amount of energy available from photosynthesis helps determine how fast the cells reach protoplasm cleavage and thus the length of time between protoplasm cleavage and cell division. This is the phase when the cells rapidly take up Si and incorporate it into the frustule. The length of this phase determines whether or not the cell has the opportunity to accumulate a large internal Si pool.

3.3 Model Validation

Following the sensitivity analysis, the model output was fitted to experimental data from three batch experiments performed by Pan and coworkers [58]. The model was calibrated to fit population size, total domoic acid in the cells and medium, and external Si concentration in experiment A. The goal was to be within 25% of the population data while capturing the dynamics of domoic acid production late in the experiment when the rate of production is highest. Since the details of DA production are not well known, we did not expect to capture perfectly the dynamics of the data associated with

it. Similarly, a qualitative fit to the external Si data was considered sufficient since the dynamics of Si uptake and deposition are probably more complex than the model representation.

The model output was first compared to data from experiment A (Figure A.11). The model described the population dynamics very well, with an average relative error of 10.9%. It was weakest in describing the tail of the stationary phase when the data showed a small increase but the model simulation did not. Upon looking at the mass of frustule for each cohort, it was determined that another reproduction was imminent in the model, therefore the model population would eventually achieve the same level as the experimental population.

For the total DA in the cells and medium, the model was successful in the first phase of domoic acid production when DA concentration is very low, and at the end of the experiment when the DA concentration reached its peak. However, the model is weakest during the transition phase, where it misses several of the data points. It may be that the cells require some time to adjust to a higher rate of DA production, which is not a requirement of the model population. If every data point was included in the error estimation, the average absolute error was 88% while omitting the third and fourth to last points yielded an average absolute error of 38%, implying that much of the error lies in those two data points. It should be noted that parameter sets resulting in outputs with errors below 20% were possible, however, model output with such a low error did not closely approximate the peak levels at the end of the experiment.

Qualitatively, the model output for external Si was similar to that of the experiment. From the data, one might infer that the cells are releasing some Si into the medium. The model does not allow for this capability, accounting for the discrepancy between the monotone decreasing curve of the model output and the experimental data which is alternatingly decreasing and increasing.

Experiment B was implemented to determine the dynamics when Si was initially

abundant in the medium (Figure A.12). Again, the population output from the model was very close to that of the experiment with an average relative error of 24%. In this experiment, the model was very close to the data at the end of the experiment, but reached the peak level much earlier than the experimental population did. The experimental population shows a slower growth rate than the model population over the period between days eight and twenty. It is possible that discrepancies in the initial population structure of the model versus the experiments may be responsible for these differences. Yet another possibility is that at these high population numbers, the cells in the experiment were affected by self-shading or other crowding factors which are not taken into account by the model.

Domoic acid levels in the model output were lower than the data in the final days of this experiment, in contrast to experiment A. However, the early phase of DA production was modelled well. Note that the model again had difficulty predicting the data in the transition phase. The average absolute error over the entire data set is 61% while omitting the transition points (fourth and fifth from last) yields an error of 33%. The lower model values at the end of the experiment are likely due to the differences between model and experimental populations mentioned above. Since the model population slows down later than the experimental population, it does not have time to produce as much DA as the experimental population.

The Si dynamics for experiment B revealed the most difference between model output and data as compared with all other experiments. The experimental population rapidly absorbed Si from the medium at the outset of the experiment, while appearing to release large amounts towards the end. It should be noted, however, that error bars for the experimental data imply that the actual amount of Si in the medium may have been much closer to zero than was measured. The low initial uptake by the model population as compared with the experimental one may occur because in the biological system, Si uptake usually occurs when cells are preparing to divide, while in the model,

the uptake is spread over the whole cycle. Therefore, if the experimental cells were in that phase when the culture was begun, they would be ready to transport large amounts of Si.

Experiment C had slightly more complex dynamics than A and B because of the addition of Si to the medium on day 14. Nevertheless, the model was able to capture much of the system dynamics (Figure A.13). Model output was very close to the population data at the beginning of the experiment and following the addition of Si to the medium. However, the model population grew much slower than the experimental population in the period immediately preceding the addition of Si to the medium. This may be attributed to differences in the model and experimental initial populations, or to the fact that the model overestimates Si limitation for low external concentrations of Si. The mean absolute error between the data and the model output was 23%.

For domoic acid production, the model underestimated the production throughout the experiment. In this experiment, cells never reach the second phase of DA production because the algae population is given Si at about the time the second phase would begin and they never make the transition to higher rates of production. Although it underestimates the amount of DA, the model curve is qualitatively similar to the data set. The model also underestimates the population data particularly between days ten and thirty, when DA production rate seems to increase slightly. This could account for the lower model values of total DA concentration.

Although the external Si dynamics showed a good qualitative fit to the data for this experiment, the period following Si addition revealed a pattern similar to that of experiment A. Silicate is most likely being excreted to some extent by the experimental cells while the model does not yet have this capability. The initial dynamics mirror the problem from experiment B where a large amount of Si is taken up immediately in the experiment but the same does not happen in the model. Again, this is likely due to differences in the two initial population structures.

3.4 Conclusions

The first set of simulations in the sensitivity analysis showed that parameters related to energy availability and Si uptake and deposition are most important to the dynamics of the population, DA and external Si. The results of the first factorial experiment were that C_E, T_1, P_{max}, and $K_{E,Pr}$ are most responsible for the observed variability in the population and Si data. C_E was particularly sensitive because it can cause the cells to die and the population to go to extinction. While energy related parameters had a greater affect on population dynamics than those related to uptake, Si data were more sensitive to the uptake parameters. The population and external Si data were closely related; therefore, we can infer that population size determines potential Si uptake and, in turn, external Si concentration. In the second factorial experiment, $M_{0,Fr}$ and C_{Si_i} appeared to influence population and Si dynamics more than P_{max} and $K_{E,Pr}$. This agrees with the fact that the experiments were set up to model a population whose dynamics are determined by the availability of Si. Domoic acid was affected by C_E, T_1, and $K_{E,Pr}$ in both of the factorial experiments. It is important that a direct link between Si parameters and DA was not established. This could mean that the correlation between DA production and external Si concentration may not be directly causal, but indirectly due to the dynamics of cell reproduction and the length of time spent in the phase between protoplasm cleavage and cell division.

Comparing the model outputs to actual data revealed some of the strengths and weaknesses of the model. The model was strongest in predicting population dynamics for various levels of external Si concentrations, with the possible exception of very low concentrations. For DA in the first and second phase, the model performed well, particularly in experiment A. However, capturing the dynamics of the transition between these two phases was one of the weaknesses of the model. Another model shortfall appeared when the model output was compared to the external Si dynamics. The fact

that the present form of the model does not allow for excretion of Si from the cells does not appear realistic in light of the experimental data which show the external Si concentration alternately increasing and decreasing.

The comparisons of model output to data also delineate the importance of the initial population structure. In experiment B, the model population grew faster than the experimental one in the period between days ten and twenty. This could be because the cells in the initial model population contained a healthy internal Si pool and were almost ready to divide. In addition, the initial external Si drops suddenly in the experimental data while a much more gradual decline was seen in the model data. If the experimental population had already reached or was close to protoplasm cleavage, a sudden uptake of Si when it became available would not be surprising because the cells would be ready to transport large amounts of Si and create the frustules of the daughter cells.

Chapter 4

Batch Culture Experiments Revisited

We hypothesize that *Pseudo-nitzschia* cells are able to adapt to low levels of external silicon by increasing their capacity for Si transport. In addition, we propose that the physiological changes required to increase uptake efficiency are positively related to domoic acid production. In order to test these hypotheses, the parameter λ_0 in the expression for $L(Si_e)$ (Equation 2.5) was chosen to be positive, thereby including a slight increase in Si uptake at low levels of Si and a correlation of the maximum DA production with $L(Si_e)$. Model output was once again compared to the three batch experiments described in Chapter 3 and improvements in the fit to total DA in cells and medium were seen. In particular, the transition period between the first and second phases of production was better represented by this form of the model.

The parameter set used for this chapter is described in Table B.17. The initial populaiton structure of the model was the same as that in the previous chapter.

4.1 Experiment A: Low initial external Si

Population dynamics were relatively unaffected by changes made to the model, and the mean relative error between model and data was 13.8% (Figure A.14). It is important to notice that the population grew much faster between days 7 and 10 and reached a higher final concentration than the population in the previous version of the model. This is due to the increased ability of the cells to transport Si even when the

concentration is very low. External Si dynamics were once again qualitatively similar to the data, although some accuracy was lost in days zero through five while some was gained between days five and twenty-five.

For DA dynamics, the improvement was significant. The average absolute error between model output and data decreased from 88% to 60% over the whole time series and from 38% to 35% when the transition points were left out. This version of the model was better able to capture the transition from the first phase to the second phase because the second phase is modeled using a variable maximum rate of production. Thus, production increases as Si uptake efficiency increases and it is possible to attain the high levels of DA observed at the end of the experiment without sacrificing accuracy during periods of lower production. This is in contrast to the previous form of the model, where either the first or the second phase could be simulated individually, but both could not be accurately represented simultaneously.

4.2 Experiment B

Model performance was most improved in Experiment B which provided high initial Si (Figure A.15). The error between the model population levels and the data decreased from 24% to 19%. The model output was especially improved in the first fifteen days of the experiment, where previously the population had been overestimated. As in experiment A, the final model population size was larger than with the previous version of the model, probably due to the increased ability for Si uptake.

External Si dynamics continued to be a challenge for this experiment. In particular, the experimental data show a large drop in external Si on day one, followed by a more gradual decrease. The model did not do well in capturing these dynamics, which may again be attributed to differences between the initial populations in the experiment and in the model. In addition, while the data show an increase in external Si after day 15, the model cells do not currently have the ability to excrete Si, therefore, external Si

can at best be a monotone decreasing curve.

The most drastic improvement over the previous version of the model was attained in the DA dynamics for this experiment. The overall average relative error in the data decreased from 61% to 36% while there was a slight increase in the error excluding the transition points from 33% to 35%. Qualitatively, the model describes the data very well, showing a long first phase of low DA production followed by a transition phase and the second phase of high production. The final amount of DA attained was approximately 60 μg/l which is a significant improvement over the previous version of the model that reached a final level of approximately 40 μg/l.

4.3 Experiment C

For experiment C there was not much improvement in the model performance (Figure A.16). This experiment is the most difficult to model because the batch culture is perturbed on day fourteen when extra Si is added. The model underestimated the population size between days five and fourteen even more than was observed in the previous version. This may be due to differences in initial populations or because the model overestimates Si limitation at moderately low levels, before uptake efficiency is increased. Once Si was added, the model population began to catch up to the data and the final population levels were almost the same.

The external Si dynamics were improved over the previous version for the period following addition of Si, but were slightly worse between days zero and fourteen. Similar to experiment B, the model did not capture the large initial drop in external Si, possibly due to discrepancies between the initial populations. In addition, the experimental Si dynamics include excretion, which the model does not.

Likely due to the low population levels in the model, DA production was very low compared to the actual data. As with the previous version of the model, DA production was underestimated but qualitatively similar in dynamics to the experimental

population. There is a slight increase in production which levels off after Si is added. As Si reaches low levels again, DA production increases.

4.4 Conclusions

The ability of algae cells to adapt to low levels of nutrient has been documented for several species [17, 18, 35, 44, 73]. We hypothesize that the same is true of *Pseudo-nitzschia* species in particular with respect to Si. In addition, the literature on DA production implies that it is negatively correlated with external Si values [58, 59]. Therefore, it is possible that the physiological changes required to increase Si transport efficiency may cause changes in the cell that increase DA production. This was implemented in the model by including the $L(Si_e)$ term in the expression for Si uptake (Equation 2.5) and also in maximum DA production (Equation 2.19). As a result, the model was better able to predict the DA dynamics throughout experiments A and B including the first and second phases of DA production and the transition phase between them.

In particular, when the second model implementation was used, the high experimental levels of DA in both experiments were modeled more accurately. These high levels were achieved without sacrificing accuracy at the beginning of the experiment when production is low. Therefore, we see that the modified model DA curve is qualitatively and quantitatively a better fit to the experimental data. These results indicate it may be possible that the cellular mechanism required to increase Si transport may be linked to the mechanism for DA production. This is one possible explanation for the correlation of DA with external Si levels, and for the fact that low levels of DA are produced consistently, but increase greatly under Si limitation.

Chapter 5

Chemostat Experiments and Nutrient Limitation

In this chapter the model is used to simulate data from continuous culture experiments and to develop criteria that govern DA production. Continuous culture experiments were performed in a chemostat, a device which allows inflow of fresh medium and outflow of mixed medium and cells. The batch and chemostat culture experiments indicate that the strain used for the chemostat experiments was better able to transport Si and other nutrients, had a higher photosynthetic rate and had a higher rate of DA production than that in the batch culture. Hence, this required the use of a modified parameter set from those used in the batch model calibration experiments. This was also verified by personal communication (Pan, 2002). In addition, the chemostat strain was able to increase Si transport efficiency to a greater degree and at a higher external Si concentration. Simulations were then performed employing a constant flow rate while increasing external Si or decreasing external N.

5.1 Biological Data

In order to study the population and DA production dynamics of *Pseudo-nitzschia multiseries*, Pan and coworkers performed a series of chemostat experiments with varying growth rates at two external Si concentrations [59]. An experiment typically describes the final steady-state of the system, which includes equilibrium population density and external nutrient concentrations. In this set of experiments, the same type

of medium was used as in the batch culture; however, the strain of *Pseudo-nitzschia multiseries* had been in culture for a shorter period of time, resulting in higher rates of DA production.

In Experiment 1, the concentration of Si in the medium was set at 165.4 μmol/l. The medium flow rate was varied between 0.10 and 0.70 per day. The data for equilibrium external Si concentration appeared to be positively linearly correlated with growth rate, while domoic acid showed a negative exponential relationship to growth rate. The authors fit curves to the data for external Si, pg DA/cell and μg DA/l in filtrate and cells. We will compare the model output to these curves (Figure A.17).

The concentration of Si in the medium for Experiment 2 was set at 56.2 μmol/l. In this experiment the cells were severely Si limited and showed very high levels of DA production. At flow rates below 0.20 d^{-1}, external Si was negatively correlated with growth rate, which the authors attributed to dissolution of Si from the cell walls of the diatoms. When the flow rate was higher than 0.20 d^{-1}, external Si levels remained unchanged indicating the equilibrium populations were Si limited. The data for pg DA/cell showed an increase until the flow rate is 0.20 d^{-1} followed by a decrease similar in pattern to the data in Experiment 1, while the total DA data appeared to also be a decreasing exponential function of growth rate. The data suggest that below the 0.20 d^{-1} flow rate, the cells were under severe stress, and were probably ceasing physiological processes. Because the model does not currently include the capability for the cell walls to dissolve or for processes to slowly cease, model output was compared to the data where the flow rates were 0.20 d^{-1} or higher.

5.2 Model Simulations

For Experiment 1, model simulations were done at 0.1 intervals starting with a flow rate of 0.2 d^{-1} and ending with 0.6 d^{-1}. Figure A.18 shows time series data for each of the flow rates. The horizontal lines represent the equilibrium value as predicted

by the fitted curves in the paper by Pan and coworkers.

Table B.15 shows the mean model output value for total DA, cellular DA, and external Si for each flow rate in experiment 1 compared with fits to experimental data performed in Pan et. al. [59]. The external Si model predictions are within 25% of the data. At higher flow rates when the cells are growing rapidly, the error improves to less than 15%. The model underestimates the cells' ability to transport Si, particularly at lower flow rates, which agrees with the results in the batch culture Experiment C, where the model population did not grow as fast as the experimental one.

For DA levels per cell the model is within 16.7% of the data with the exception of the experiment performed at flow rate 0.6d^{-1} where the relative error is large. However, it is important to note that the model output is within 0.04 of the data, therefore the seemingly large error is due to the very low levels of DA present. The results are similar for total DA in cells and medium, where the error is within 35.6% excepting the higher error at the 0.6d^{-1} flow rate. The main concern is to model the dangerous high levels of DA that may occur, and the data suggest that the model successfully accomplishes this goal.

Simulations for Experiment 2 were performed at growth rates of 0.2 d^{-1}, 0.3 d^{-1} and 0.4 d^{-1} (Figure A.19). It should be noted that all the parameter values were kept constant between Experiment 1 and 2 except for the amount of frustule required for reproduction. Cells in Experiment 2 were allowed to have 35% less Si in their frustules than those of Experiment 1. This was necessary for the population to be able to persist at a growth rate of 0.4 d^{-1}. This is a justifiable change, since under Si stress diatoms may use less Si to form their frustules.

For this experiment, the errors between model output and data were higher than in Experiment 1 (Table B.16). For the equilibrium values of DA/cell the highest error was 41.5%, and for total DA the highest error was 57.8%. It should be noted, however, that model predictions for DA/cell were at worst 2.2 pg from the actual data. The

error for total DA implies the model population was larger than the experimental one, resulting in an overestimation of the total DA in the system. For external Si the relative errors are extremely high. However, the model output is at worst within 6 μmoles of the data. Considering the range of Si values from almost 100 μmoles/l to 2 μmoles/l, the model does well to be so close to levels ranging over 2 orders of magnitude.

5.3 Comparison of Batch and Chemostat culture strains

The sets of batch and chemostat experiments were performed on two different strains of *Pseudo-nitzschia multiseries*. The strain used for the batch culture experiments had been in culture for a long period of time, resulting in a loss of vitality and particularly a loss of ability to produce DA. Therefore, two separate parameter sets were required to model the two sets of experiments. Differences in these parameter sets may reveal the physiological differences between the algae strains. It is important to note, however, that since both sets of experiments were performed to explore Si limitation, parameters related to other nutrients did not change in the model. This should not be taken to imply that there is no difference between the two strains' ability to transport N or P, but simply that this aspect of cell physiology was not explored in these experiments.

The main differences in the parameter sets are between parameters related to uptake. For all nutrients, the value of the parameter S (Equation 2.2), the velocity at which a nutrient is passed through the cell membrane at the reference temperature, for the chemostat experiments was approximately four times that of the batch experiments. Therefore the "younger" chemostat cells were able to transport nutrient from the medium into the cell much faster than those in the batch culture. The parameters specific to Si uptake showed the same trend. The number of transport sites for Si, $n_{Si,e}$ (Equation 2.5) in the chemostat cells used was twice that of the batch cells resulting in a higher maximum rate of uptake. The differences in the proportionality constant

c_{Si} result in a higher half saturation constant for the chemostat culture than for the batch culture. Thus, while the strain used for the chemostat experiments has a higher maximum uptake rate, it reaches that rate slower than the batch culture will reach its maximum rate of uptake. Regardless of this difference, the uptake rate of Si over the entire experimental range is still higher for the chemostat strain.

The strain used for the chemostat model also shows a greater ability to increase the efficiency of Si uptake when Si is limiting (Figure A.20). The chemostat strain begins increasing uptake efficiency at approximately 25 μmols external Si/L while the batch strain does so only at approximately 8 μmols external Si/L. In addition, the strain used in the chemostat shows a greater overall increase in efficiency at low levels of external Si, although the batch culture strain is able to increase efficiency more dramatically at low levels of external Si.

In addition to differences in uptake there were a few more physiological differences between the two strains. The chemostat strain had a higher maximum photosynthetic rate than the batch culture strain, but there were no changes in the other photosynthesis parameters. The maximum rate of DA production was approximately 17 times higher for the chemostat strain. This may seem unreasonable at first, but such a large difference is reflected in the data for the two experiments. Finally, the maximum rate of production for protein was approximately 50% higher for the cells in the chemostat. Since the strain used for the chemostat experiments was chosen because it would be more vigorous, these differences are not surprising.

There were some parameter differences that are difficult to explain biologically. The chemostat cells had a lower maximum production rate of frustule than the batch cells and the wait times for nutrients were also much larger than in the batch culture. Intuitively, the opposite should be true in both cases. This may indicate a weakness of the model. However, simulations where the wait time was decreased resulted in the population going to extinction because the cells became energy deficient. Therefore,

these differences may be due to the fact that when the cell has an abundance of available nutrients, it doesn't use them as quickly so that energy is not depleted too rapidly.

5.4 Toxin production simulations

Given that the model has been calibrated to fit experimental data, it is a logical next step to use the model to characterize nutrient regimes likely to cause toxin production, while examining internal cell physiology to gain insight into the internal factors that may be governing production. Thus, simulations using a single cohort were performed so that all cells would be synchronized and their physiological characteristics would be easy to discern. Domoic acid per cell was used as the response variable so that increases or decreases in DA concentration due to population size would be ruled out.

The external conditions in the model were made to mimic chemostat Experiment 2 with a flow rate of 20%day^{-1}, which represented the highest toxin production of all the experiments performed. Two sets of simulation experiments were done. In the first set of experiments, the concentration of Si in the medium was increased gradually while in the second set the external concentration of N was decreased gradually. Thus, we can investigate the situation where Si was not limiting, in addition to the situation where both Si and N were limiting. The biological data suggest that in both these scenarios, toxin production is low.

In the base case where external Si was set at 56.2 μmol/l as in the original experiment, the DA per cell increased rapidly and then stabilized at levels between four and eight pg per cell. The level fluctuates between these two values since at each cell division, all internal components of the cell including DA are halved (Figure A.21). Throughout this simulation, Si is obviously a limiting factor, as demonstrated by the very low levels of Si available in the cells' nutrient pool, while the model indicates that the limiting factor for protein production is energy. Thus, cell growth is not limited by either N or P.

A gradual increase in Si in the medium produced the expected result of lowering toxin production. DA per cell did not change as the Si concentration was raised to 1375 μmol per liter. However, at 1405 μmol per liter, the concentration of DA per cell began to show a cyclical pattern which was observed at Si levels up to 1465 μmol/l. The cycle is characterized by periods of high DA production followed by periods where almost no production occurs. As Si concentration increases, the period of high production becomes shorter (Figure A.22). The periods of low production are characterized by N limited protein production, while the periods of high production are energy limited as in the simulations with low levels of Si. This implies that Si is no longer limiting during the periods of high DA production and cell growth and division is controlled by the amount of N available for protein production. Figure A.23 shows one example of a simulation where DA/cell dynamics are cyclical and indicate periods of N limited protein production corresponding to low DA production.

When Si concentrations are raised to 1500 μmols or higher, DA/per cell stabilizes at levels between 0.01 pg/cell and 0.02 pg/cell after an initial spike of high production (Figure A.24). The internal dynamics of the cell indicate that the cell growth and division are now exclusively N limited, so that the cell no longer lingers in the phase between protoplasm cleavage and division. In addition, the N pool is sufficiently depleted by protein production leaving little available N to build DA molecules.

The simulations where external N concentration was lowered showed similar results to those above. Initially there were 1765 μmols N /L in the medium. The DA dynamics remain the same until external N reaches 65 μmol/L. At this point, the same type of cyclical behavior is observed, with periods of high DA production followed by periods of low production. As N was further lowered, the periods of high production became shorter, and the peak levels of DA/cell decreased (Figure A.25). The internal physiology of the cell again indicated that times of low production were characterized by N limitation (Figure A.26). Finally, as N became the sole limiting nutrient, DA

production was very low even though the cells were also in a medium of low Si concentration.

The results of these simulations indicate that N plays as important a role as Si in DA production. When cells are in an Si rich environment, they produce very little DA, possibly because the cells are growing rapidly enough so that there is no excess N to be used in the formation of DA molecules. On the other hand, when Si is limiting we have two scenarios. Either there is abundant N in the medium and high levels of DA production are possible, or the cells can also be starved for N in which case DA production will be low. Therefore it is necessary to have the combination of low Si and high N in order to get high levels of DA production. In addition, this may imply that the production of DA can be a mechanism to rid the cell of excess N.

Of particular interest are the nutrient regimes where the cells are alternately Si and N limited, which are characterized by cyclic production rates. This is a phenomenon not likely to be observed in nature since the algae population will not be composed of identical cells. Thus, the model gives us some insight as to the possibility that there are nutrient regimes which in nature may or may not produce high levels of DA, depending on the population structure of the algae population.

5.5 Conclusions

The model was successful at describing the dynamics of the chemostat experiments performed by Pan and coworkers. This, combined with the results for the batch cultures in Chapter 4, provides a measure of confidence in using the model as a tool to make inferences about the biological condition of the cells as they grow and produce domoic acid in different environmental situations.

The two different strains used in the batch and chemostat cultures likely differed in their ability to take up nutrients, photosynthesize, and produce DA. The parameter differences required in the model to simulate both sets of experiments imply that overall

nutrient uptake is higher for the newer strain used in the chemostat experiments, likely due to a more efficient mechanism for transport of nutrients through the cell membrane. In addition, the chemostat culture had more active uptake sites for Si as well as an enhanced ability to adapt to low Si levels. It can not be determined whether there are differences in the cells' ability to take up other nutrients, since those data were not available. Higher maximum photosynthetic rate and maximum DA production rate were the final parameters that made the difference between the performance of the cells in the batch culture and those of the chemostat culture.

The simulations performed to investigate DA production showed that both N and Si play an important role in DA production. Simulations where both Si and N were limiting produced very little DA, while those under exclusive Si limitation showed high levels of production. In addition, when the shift from Si to N limitation occurred, DA production was very low. Particularly telling were the simulations where the limitation alternated between Si and N. These simulations showed that during periods of N limitation, DA production was low, while high periods of production coincided with periods of Si limitation. It has also been shown in experiments that cells limited by P produce higher levels of DA. Therefore, not only does DA production require N, it may be a mechanism for the cell to rid itself of excess N.

Chapter 6

Summary of Results and Future Directions

The model presented in this work shows promise as a tool for biologists and modelers alike. It is contemporary in formulation by employing stoichiometry and in application to harmful algae blooms. Since the sensitivity analysis results appeared to agree with the expectations for the experiment being modeled and model outputs matched two sets of experiments well, we are justified in using the model as a tool to gain insight into the dynamics and physiology of DA production.

The sensitivity analysis results showed that the parameters most affecting population dynamics were energy and Si related. Because the experiments being reproduced in the simulations were designed to characterize dynamics under Si limited conditions, this is a logical result. In addition, DA appeared to be related to parameters determining the length of time the cell remained in the phase immediately preceding division when the frustules of the daughter cells are built.

When compared with experimental data from batch experiments, the model results appeared to describe the dynamics of population growth and DA production quantitatively well. The dynamics of external Si were more difficult to capture, but qualitatively, the model was adequate. Results for DA production were dramatically improved when the model cells were given the capability to adapt to low levels of external Si by increasing their uptake efficiency. When the maximum rate of DA production was also related to Si transport efficiency, the model results captured both the high levels of DA

observed at the end of each experiment, and the low levels of production associated with the early stages of each experiment. This may imply that a high affinity transport system takes effect at low levels of external Si which is activated by a genetic or physiological switch. This switch can also be responsible for increased DA production by the cell. Alternatively, there may be other physiological changes in the cell associated with increased Si transport efficiency which increase DA production. This hypothesis could be tested experimentally by determining whether or not *Pseudo-nitzschia multiseries* has the capapbility of activating a high-affinity transport system. If it does have this capability, then DA production when the system is active can be compared to Da production when it is not active to determine whether there is a link between the two.

The model may also be used to gain insight into the differences between two strains of algae, as was done in Chapter 5. Two different strains were used in the batch and chemostat experiments, therefore two different parameter sets were required to accurately model the biological data. The differences between these two data sets reveal that the older strains may lose some of their ability to take up nutrients, resulting in a less vigorously growing population. In addition, they may also have more difficulty adapting to low nutrient levels by increasing transport efficiency in periods of nutrient limitation. The parameters imply that this is true of Si uptake dynamics, but we cannot make a conjecture about N and P uptake since data for situations in which those nutrients were limiting were not available. The other parameter differences reveal that older strains have lower maximum photosynthetic rates and maximum DA production rates than fresher ones. Again, these hypotheses are testable in the laboratory by comparing uptake and photosynthetic rates for two strains, one that has been in culture for a long period of time, and one that has not.

Finally, we have demonstrated that available N is an important factor in DA production (Table B.18). Simulations that were Si limited, but had abundant N, produced high levels of DA, while in the absence of N, DA production was very low. This is due

to the fact that the cell does not have excess N with which to construct DA molecules. On the other hand, as external Si increases, DA production begins to decrease when N begins to become the limiting nutrient to cell growth and division. This may imply that the cells produce DA as a mechanism for removal of excess N. In addition, there are some interesting nutrient regimes where the cells can alternate between being N and Si limited. In the former, little DA is produced, while more is produced in the latter. It appears that the switch between N and Si limitation may be yet another factor that turns on DA production.

6.1 Future Directions

The possibilites for future research and improvements to the model are many. First, some improvements can be made to the model in order to better describe the *Pseudo-nitzschia* species and its toxin production. Second, model simulations that include factors such as P limitation, temperature, and light could be performed to further investigate population and DA dynamics. In addition, the approach could be adapted to other toxic algae species.

While nutrient-uptake dynamics seem to be adequate, the model lacks a mechanism for the excretion of Si or its dissolution from the frustule back into the environment. One of the weak points of the model conclusions was the high error observed between model output and external Si data for batch culture. This was largely due to the fact that the data showed periods where the external Si concentration increased, but the model did not afford that possibility. Also it would be illustrative to compare model outputs to experiments performed under P limitation. Currently, all biological data was based on Si limitation, so that parameters affecting P and N were not sensitive and therefore not fully explored. Continuing to experiment with model outputs and comparing them to biological data may result in more accurate parameter values for the model. This would constitute another step toward making the model more biologically

realistic.

With these goals accomplished, it would then be possible to more fully investigate nutrient regimes likely to cause high levels of DA production. In addition, DA production due to P limitation could be further explored. Finally, it would be interesting to do long term simulations to explore the effect of sexual reproduction on toxin production as well as size distribution of the population. This may lead to hypotheses surrounding the observation that smaller cells tend to produce less DA than younger, larger cells.

Another step towards greater understanding of DA production would be the coupling of the existing algae model with a bacterial model. The symbiotic relationship between plants and bacteria is well documented [64], and in the case of *Pseudo-nitzshia* species it has been demonstrated in the laboratory that cells produce much more DA in the presence of their associated bacteria than when the bacteria are removed from the culture [4, 5].

Currently the model is a good tool for simulations describing laboratory experiments. However, in order to model natural populations it would require that spatial heterogeneity be incorporated. It would be useful to couple the model with a physical model that described the currents, shear and upwelling occurring in a natural environment.

Finally, minor changes are required to adapt the model to other toxin-producing algae species. This would serve at least two purposes. The first would be to imitate the types of simulations done here on *Pseudo-nitzschia* species in an attempt to characterize the driving forces of population and toxin production dynamics for other species. Secondly, it would be interesting if certain parallel behaviors could be discerned in order to shed light on the problem of toxin-producing algae.

Bibliography

Bibliography

[1] John W. Anderson and John Beardall. Molecular Activities of Plant Cells. Blackwell Scientific Publications, Boston, 1991.

[2] S.S. Bates, C.J. Bird, A.S.W. de Freitas, R. Foxall, M. Gilgan, L.A. Hanic, G.R. Johnson, A.W. McCulloch, P. Odense, R. Pocklington, M.A. Quilliam, P.G. Sim, J.C. Smith, D.V. Subba Rao, E.C.D. Todd, J.A. Walter, and J.L.C. Wright. Pennate diatom *Nitzschia pungens* as the primary source of domoic acid, a toxin in shellfish from Eastern Prince Edward Island, Canada. Can. J. Fish. Aquat. Sci., 46:1203–1215, 1989.

[3] S.S. Bates, A.S.W de Freitas, J.E. Milley, R. Pocklington, M.A. Quilliam, J.C. Smith, and J. Worms. Controls on domoic acid production by the diatom *Nitzschia pungens* f. *multiseries* in culture: nutrients and irradiance. Can. J. Fish. Aquat. Sci, 48:1136–1144, 1991.

[4] S.S. Bates, D.J. Douglas, G.J. Doucette, and C. Leger. Effects of reintroducing bacteria on domoic acid production by axenic cultures of the diatom *Pseudonitzschia pungens* f. *multiseries* . In Harmful Marine Algal Blooms. Lavoisier, Paris, France, 1995.

[5] S.S. Bates, D.J Douglas, G.J. Doucette, and C. Leger. Enhancement of domoic acid production by reintroducing bacteria to axenic cultures of the diatom *Pseudonitzschia multiseries* . Nat. Tox., 3:428–435, 1995.

[6] S.S. Bates, D.L. Garrison, and R.A. Horner. Bloom dynamics and physiology of domoic acid producing *Pseudo-nitzschia* species. In The Physiological Ecology of Harmful Algal Blooms. Springer-Verlag, Heidelberg, 1997.

[7] S.S. Bates, C. Leger, and K.M. Smith. Domoic acid production by the diatom *Pseudo-nitzschia multiseries* as a function of division rate in silicate-limited chemostat culture. In Harmful and Toxic Algal Blooms. UNESCO, Paris, 1996.

[8] S.S. Bates, J. Worms, and J.C. Smith. Effects of ammonium and nitrate on domoic acid production by *Pseudonitzschia pungens* in batch culture. Can. J. Fish. Aquat. Sci, 50:1248–1254, 1993.

[9] A.P. Belov. A model of phycotoxin release by cyanobacterial cells. Ecol. Mod., 100:105–117, 1998.

[10] C.J. Bird and L.J.C Wright. The shellfish toxin domoic acid. World Aquaculture, 20:40–41, 1989.

[11] G.S. Blank and C.W. Sullivan. Diatom mineralization of silicic acid. Arch. Microbiol, 123:157–164, 1979.

[12] H. C. Bold and M. J. Wynne. Introduction to the Algae: Structure and Reproduction. Prentice Hall, New Jersey, 1985.

[13] M. R. Brown. The amino acid and sugar composition of 16 species of microalgae used in mariculture. J. Exp. Mar. Biol. Ecol., 145:79–99, 1991.

[14] M. A. Brzezinski, R. J. Olson, and S. W. Chisholm. Silicon availability and cell-cycle progression in marine diatoms. Mar. Ecol. Prog. Ser., 67:83–96, 1990.

[15] D. Cannon. State reports: Oregon. West Coast Marine Biotoxins and Harmful Algal Blooms Newsletter, 1998. NOAA.

[16] E. E. Conn and P.K. Stumpf. Outlines of Biochemistry. John Wiley and Sons, Inc., New York, 1972.

[17] H. Conway and P. Harrison. Marine diatoms grown in chemostats under silicate or ammonium limitation iv. transient response of *chaetoceros debilis*, *skeletonema costatum* and *thalassiosira gravida* to a single addition of the limiting nutrient. Mar. Biol., 43:33–43, 1977.

[18] F. Daniel-Vedele, S. Filleur, and M. Caboche. Nitrate transport: a key step in nitrate assimilation. Curr Opin Plant Biol, 1(3):235–239, 1998.

[19] N. A. Davidovich and S. S. Bates. Sexual reproduction in the pennate diatoms *Pseudo-nitzschia multiseries* and *p. Pseudodelicatissima* (bacillariophycae). J. Phycol, 34:126–137, 1998.

[20] R. P. Desai, L. K. Nielsen, and E. T. Papoutsakis. Stoichiometric modeling of *clostridium acetobutylicum* fermentations with non-linear constraints. J. Biotech., 71:191–205, 1999.

[21] K. M. Donald, D.J. Scanlan, N.G. Carr, N.H. Mann, and I. Joint. Comparative phosphorus nutrition of the marine cyanobacterium *Synecoccus* wh7803 and the marine diatom *Thalassiosira weisflogii. J. Plank. Res., 19(12):1793–1813, 1997.*

[22] D.J. Douglas, S.S. Bates, L.A. Bourque, and R. Selvin. Domoic acid production by axenic and non-axenic cultures of the pennate diatom Nitzschia pungens f. *multiseries.* In Toxic Phytoplankton Blooms in the Sea. Elsevier Sci. Publ. B.V., Amsterdam, 1992.

[23] W. Ebenhoh. Coexistence of a limited number of algal species in a model system. Theor. Pop. Biol., 34:130–144, 1988.

[24] J.J. Elser, D.R. Dobberfuhl, N. A. MacKay, and J.H. Schampel. Organism size, life history and N:P stoichiometry. Bioscience, 46(9):674–684, 1996.

[25] I.R. Falconer, editor. Algal Toxins in Seafood and Drinking water. Academic Press, San Diego, 1993.

[26] K. J. Flynn, M. J.R. Fasham, and C. R. Hipkin. Modelling the interactions between ammonium and nitrate uptake in marine phytoplankton. Phil. Trans. R. Soc. Lond. B, 352:1625–1645, 1997.

[27] K.J. Flynn. Physiology of toxic microalgae with special emphasis on toxin production: construction of dynamic models. In Harmful Algae. Xunta de Galicia and Intergovernmental Oceanographic Comission of UNESCO, Galicia, 1998.

[28] K.J. Flynn and K. Flynn. Release of nitrite by marine dinoflagellates: development of a mathematical simulation. Mar. Biol., 130:455–470, 1998.

[29] P.J.S. Franks. Models of harmful algal blooms. Limnol. Oceanogr., 42(2):1273–1282, 1997.

[30] L. Fritz, M.A. Quilliam, J.L.C. Wright, A. Beale, and T.M. Work. An outbreak of domoic acid poisoning attributed to the pennate diatom *Pseudonitzschia australis*. J. Phycol., 28:439–442, 1992.

[31] P. Gentien. Report of the ICES-IOC Working Group in Harmful Algal Bloom Dynamics. Technical report, International Council for the Exploration of the Sea, 1999.

[32] B.S. Guttman. Biology. McGraw-Hill, Boston, 1999.

[33] G.M.A. Hallegraeff. A review of harmful algal blooms and their apparent global increase. Phycologia, 32(2):79–99, 1993.

[34] L.D. Hanson. State reports: Washington. West Coast Marine Biotoxins and Harmful Algal Blooms Newsletter, 1998. NOAA.

[35] P.J. Harrison, R. Holmes, and C.O. Davis. Marine diatoms grown in chemostats under silicate or ammonium limitation iii. cellular chemical composition and morphology of *chaetoceros debilis*, *skeletonmea costatum* and *thalassiosira gravida*. Mar. Biol., 43:19–31, 1977.

[36] H. Hillebrand and U. Sommer. Nitrogenous nutrition of the potentially toxic diatom *Pseudonitzschia pungens* f. *multiseries* hasle. J. Plank. Res., 18(2):295–301, 1996.

[37] R.A. Horner and J.R. Postel. Toxic diatoms in Western Washington waters (U.S. West coast. Hydrobiologia, 269:197–205, 1993.

[38] A. Howard, M.J. Kirby, P.E. Kneale, and A.T. McDonald. Modeling the growth of cyanobacteria (growscum). Hydrol. Proc., 9:809–820, 1995.

[39] J. Hurlebaus. An individual-based model for phytoplankton assemblages with application to *Skeletonema costatum* . Master's thesis, University of Tennessee, Knoxville, 1997.

[40] G.E. Hutchinson. The paradox of the plankton. Am. Nat., 95:137–145, 1961.

[41] Harmful Algae News, November 2000.

[42] F. Iverson and J. Truelove. Toxicology and seafood toxins: domoic acid. Nat. Toxins, 2:334–339, 1994.

[43] A. E. Jackson, S. W. Ayer, and M. V. Laycock. The effect of salinity on growth and amino acid composition in the marine diatom *Nitzschia pungens*. Can. J. Bot., 70:2198–2201, 1992.

[44] M. Jansson. Uptake, exchange, and excretion of orthophosphate in phosphate starved *Scenedesmus quadricauda* and *Pseudomonas* K7. Limnol. Oceanogr., 38(6):1162–1178, 1992.

[45] D. Kamykowski. Possible interaction between phytoplankton and semidiurnal internal tides. Jour. Mar. Res, 32(1):67–89, 1974.

[46] D. Kamykowski. The growth response of a model *Gymnodium splendens* in stationary and wavy water columns. Mar. Biol., 50:289–303, 1979.

[47] B. Kennedy. Scots skippers count the cost of scallop ban, buildup of toxins sparked action. Press and Journal, July 13, 1999.

[48] H. Kierstead and L.B. Slobodkin. The size of water masses containing plankton blooms. J. Mar. Res, 7(1):141–147, 1953.

[49] M. Kishi and S. Ikeda. Population dynamics of 'red tide' organisms in eutrophicated coastal waters - numerical experiment of phytoplankton bloom in the East Seto Inland Sea, Japan. Ecol. Mod., 31:145–174, 1986.

[50] K. Kishimoto. Coexistence of any number of species in the Lotka - Volterra competitive sytem over two patches. Theor. Pop. Biol., 38:149–158, 1990.

[51] S.A.L.M. Kooijman, B.W. Kooi, and T.G. Hallam. The application of mass and energy conservation laws in physiologically structured population models of heterotrophic organisms. J. Theor. Biol, 197:371–192, 1999.

[52] G.W. Langlois and S. Loscutoff. State reports: California. West Coast Marine Biotoxins and Harmful Algal Blooms Newsletter, 2000. NOAA.

[53] I. Loladze, Y. Kuang, and J. J. Elser. Stoichiometry in producer-grazer systems: Linking energy flow with element cycling. Bull. Math. Biol., 62:1137–1162, 2000.

[54] D. J. MacPhee, L.A. Hanic, D.L. Friesen, and D.E. Sims. Morphology of the toxin-producing diatom *Nitzschia pungens* grunow forma *multiseries* hasle. Can. J. Fish. Aquat. Sci., 49:303–311, 1992.

[55] E. M. Miller. Analysis and parallel implementation of an individually-based algae model. Master's thesis, University of Tennessee, Knoxville, 1999.

[56] T. Yu Orlova, N.V. Zhukova, and I.V. Stonik. Bloom forming diatom *Pseudonitzschia pungens* in amurskii bay (the sea of japan): Morphology, ecology, and biochemistry. In Harmful and Toxic Algal Blooms. Intergovernmental Oceanographic Commission, UNESCO, Paris, 1996.

[57] M. Osada and J.E. Stewart. Gluconic acid/gluconolactone: physiological influences on domoic acid production by bacteria associated with *Pseudo-nitzschia multiseries*. Aquat. Microb. Ecol., 12:203–209, 1997.

[58] Y. Pan, D.V. Subba Rao, D.H. Mann, R.G. Brown, , and R. Pocklington. Effects of silicate on production of domoic acid, a neurotoxin, by the diatom *Pseudo-nitzschia multiseries*.I. Batch culture studies. Mar. Ecol. Prog. Ser., 131:225–233, 1996.

[59] Y. Pan, D.V. Subba Rao, D.H. Mann, W.K.W. Li, and W.G. Harrison. Effects of silicate limitation on production of domoic acid, a neurotoxin, by the diatom *Pseudo-nitzschia multiseries.* II. continuous culture studies. Mar. Ecol. Prog Ser., 131:235–243, 1996.

[60] Y. Pan, D.V. Subba Rao, and K.H Mann. Acclimation to low light intensity in photosynthesis and growth of *Pseudo-nitzschia multiseries* hasle, a neurotoxigenic diatom. J. Plank. Res., 18(8):1427–1438, 1996.

[61] Y. Pan, D.V. Subba Rao, and K.H Mann. Changes in domoic acid production and cellular chemical composition of the toxigenic diatom *Pseudo-nitzschia multiseries* under phosphate limitation. J. Phycol., 32:371–381, 1996.

[62] Y. Pan, D.V. Subba Rao, and R.E. Warnock. Photosynthesis and growth of *Nitzschia pungens* f. *multiseries* hasle, a neurotoxin producing diatom. J. Exp. Mar. Biol. Ecol., 154:77–96, 1991.

[63] C.C. Parrish, A.S.W. DeFreitas, G. Boddenec, and E.J. Macpherson. Lipid composition of the toxic marine diatom, *Nitzschia pungens* . Phytochemistry, 30(1):113–116, 1991.

[64] E.J. Patriarca, R. Tate, and M. Iaccarino. Key role of bacterial nh4+ metabolism in rhizobium-plant symbiosis. Microbiol Mol Biol R, 66(2):203, 2002.

[65] T. Platt, C.L. Gallegos, and W.G. Harrison. Photoinhibition of photosynethesis in natural assemblages of marine phytoplankton. J. Mar. Res., 38:687–701, 1980.

[66] E. Rabinowitch and Govindjee. Photosynthesis. John Wiley and Sons, New York, 1969.

[67] P. Raimbault. Influence of temperature on the transient response in nitrate uptake and reduction by four marine diatoms. J. Exp. Mar. Biol. Ecol., 84:37–53, 1984.

[68] A. Redfield, B. Ketchum, and F. Richards. The influence of organisms on the composition of sea water. In The Sea. Academic Press, New York, 1963.

[69] W. A. Reiners. Complementary models for ecosystems. Am. Nat., 127(1):59–73, 1986.

[70] J. E. Stewart, L.J. Marks, C.R. Wood, S.M. Risser, and S. Gray. Symbiotic relations between bacteria and the domoic acid poducing diatom *Pseudo-nitzschia multiseries* and the capacity of these bacteria for gluconic acid/gluconolactone formation. Aquat. Microb. Ecol., 12:211–221, 1997.

[71] C. W. Sullivan and B.E. Volcani. Silicon in the cellular metabolism of diatoms. In Silicon and Siliceous Structures in Biological Systems. Springer-Verlag., New York, 1981.

[72] C.W. Sullivan. Diatom mineralization of silicic acid. II. regulation of $Si(OH)_4$ transport rates during the cell cycle of *Navicula pelliculosa*. J. Phycol., 13:86–91, 1977.

[73] D. Tilman and S.S. Kilham. Phosphate and silicate growth and uptake kinetics of the diatoms *astrionella formosa* and *cyclotella meneghiniana* in batch and semicontinuous culture. J. Phycol., 12:375–383, 1976.

[74] E.C.D. Todd. Domoic acid and amnesic shellfish poisoning - a review. J. Food Prot., 56(1):69–83, 1993.

[75] J.E. Truscott. Environmental forcing of simple plankton models. J. Plank. Res., 17(12):2207–2232, 1995.

[76] Fish and shellfish ban in Morro Bay. Web Page. http://www.planetexpansion.org/ban.html.

[77] T. Wyatt and J. Horwood. Model which generates red tides. Nature, 244:238–240, 1973.

Appendices

Appendix A

Figures

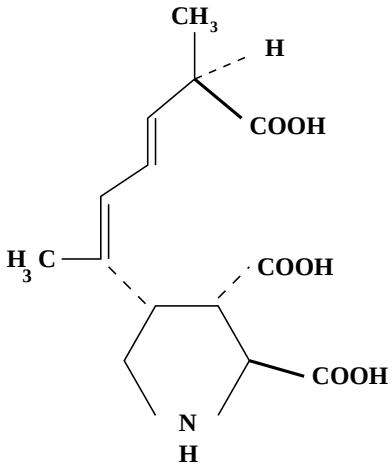

Figure A.1: The Domoic Acid Molecule. Domoic acid is a neurotoxic amino acid.

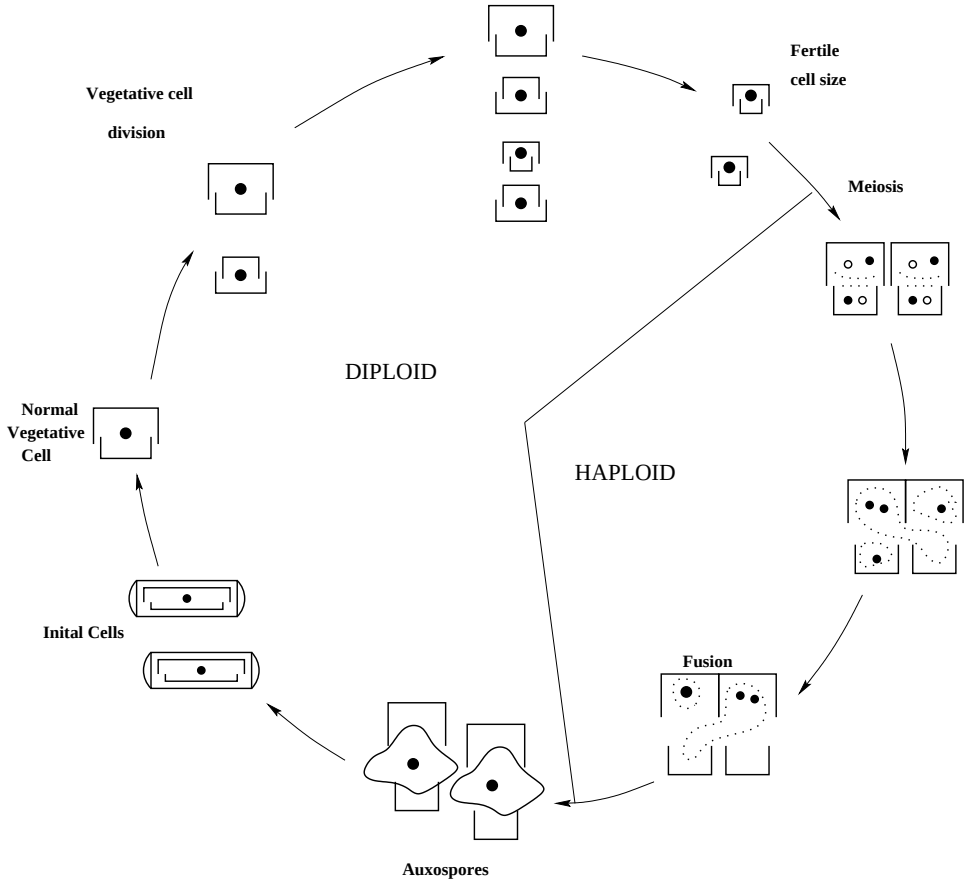

Figure A.2: Diatom life cycle [32]

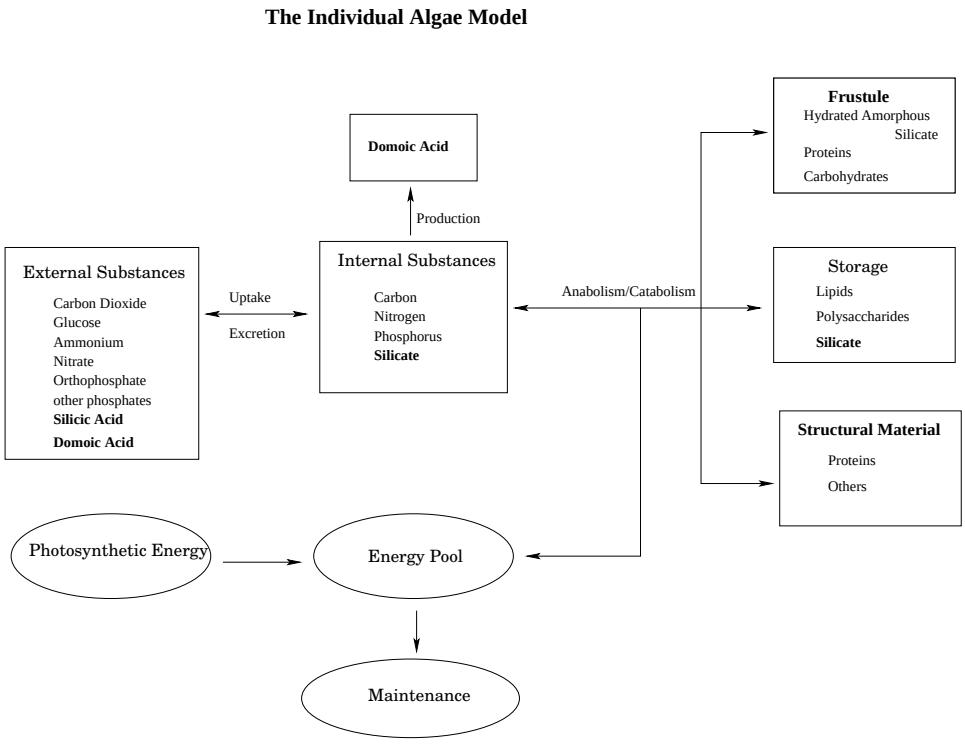

Figure A.3: The Individual Model. Items in bold denote model changes since Hurlebaus [39] and Miller [55].

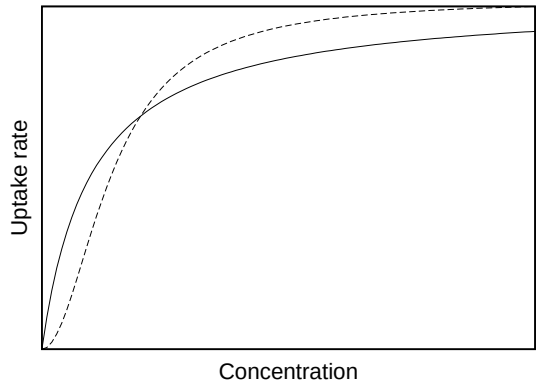

Figure A.4: Two functional forms for nutrient uptake with $M = 10$ and $k = 2$. The solid line is the classic Michaelis-Menten form, the dashed line takes the form of Equation 2.4

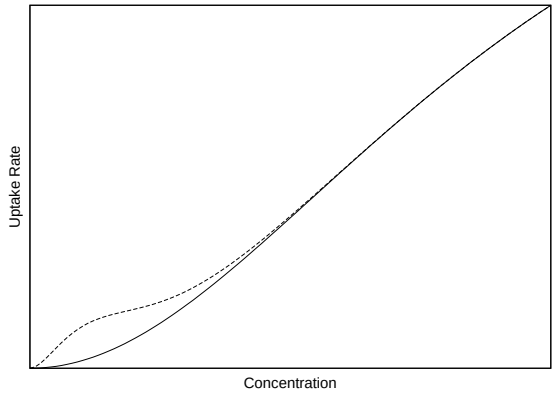

Figure A.5: Two forms of silicon uptake rate. Solid line shows uptake rate without added effiency and dashed line shows uptake rate with added efficiency. The curve is shown for low concentrations, $M = 10$, $k = 2$, $\lambda_0 = 20$, and $\rho = 10$.

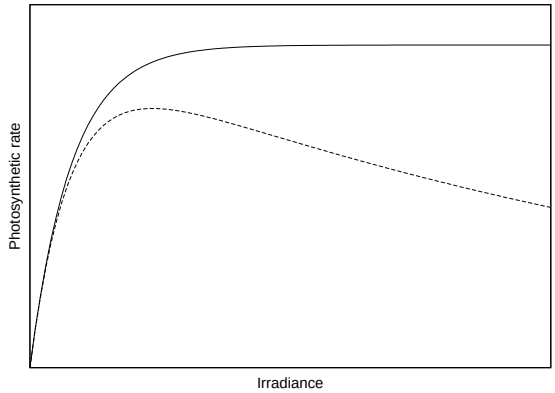

Figure A.6: The photosynthesis-irradiance curve of Platt et. al. [65] with (dashed line) and without (solid line) photoinhibition. Parameter values for this graph are $P_{max} = 8.0 \times 10^{-3}$, $\alpha = 5.0 \times 10^{-5}$, and $\beta = 2.8 \times 10^{-6}$

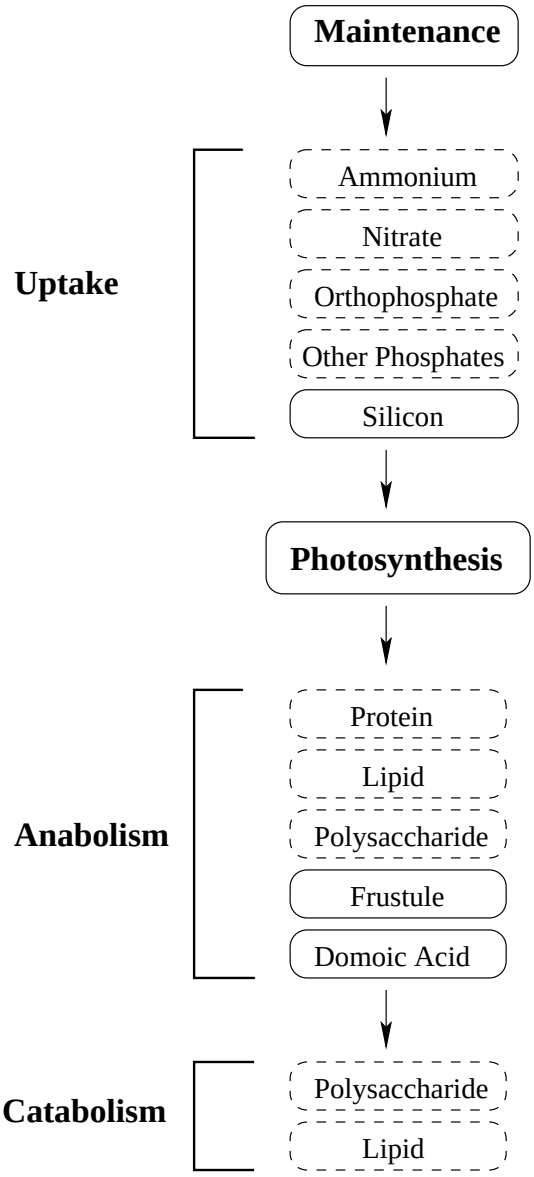

Figure A.7: Individual Model: Implementation and order of processes. Processes contained in the dashed boxes do not occur if protein has doubled.

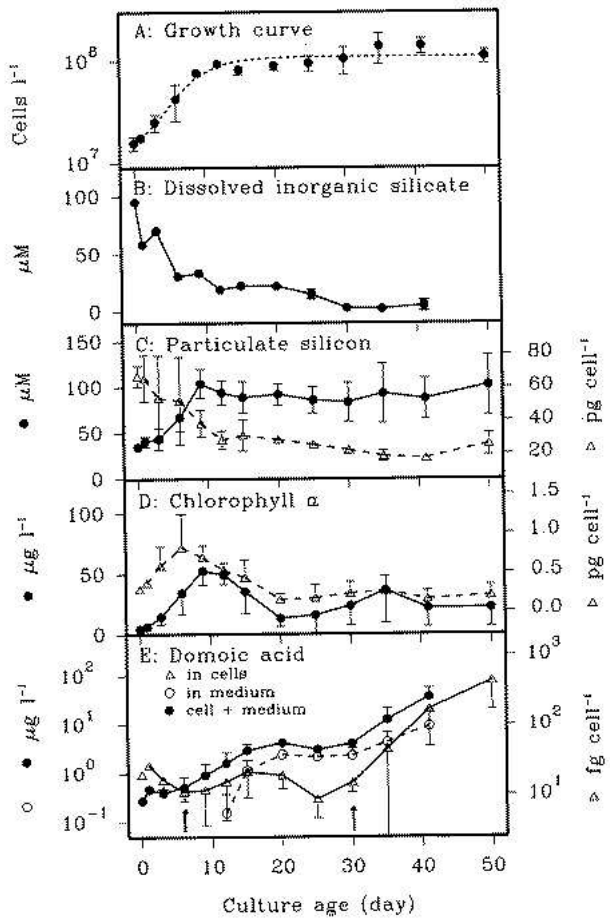

Figure A.8: Data from batch Experiment A, recreated from Pan et al. [58]. Graph A shows cell concentration, Graph B shows dissolved inorganic silicate, Graph C shows particulate Si in the medium and in the cells, Graph D shows chlorophyll a concentration, and Graph E shows domoic acid concentration in the cells, in the medium, and in total. Error bars represent one standard deviation. If there is no error bar, the standard deviation is smaller than the symbol. In graph A, the curve represents a fitted Gompertz model. Arrows in E show the onset of stage 1 and stage 2 of DA production.

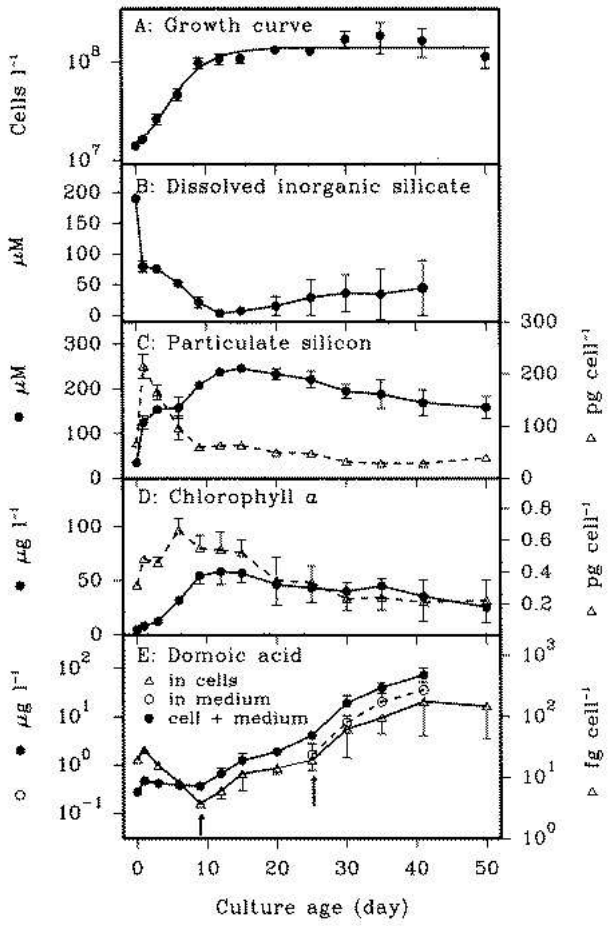

Figure A.9: Data from batch Experiment B, recreated from Pan et al. [58]. Description as in Figure A.8

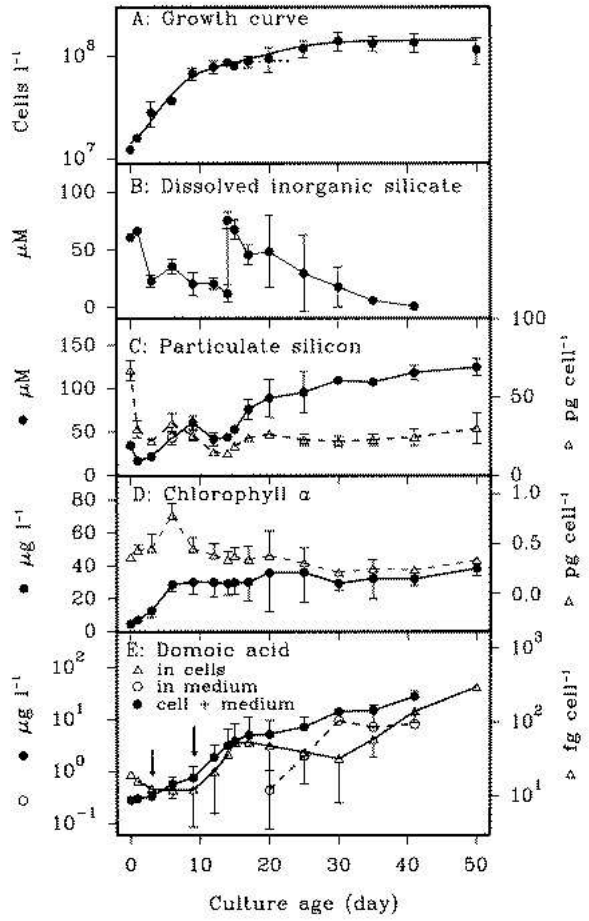

Figure A.10: Data from batch Experiment C, recreated from Pan et al. [58]. Note the addition of silicate on day 14. Description as in Figure A.8.

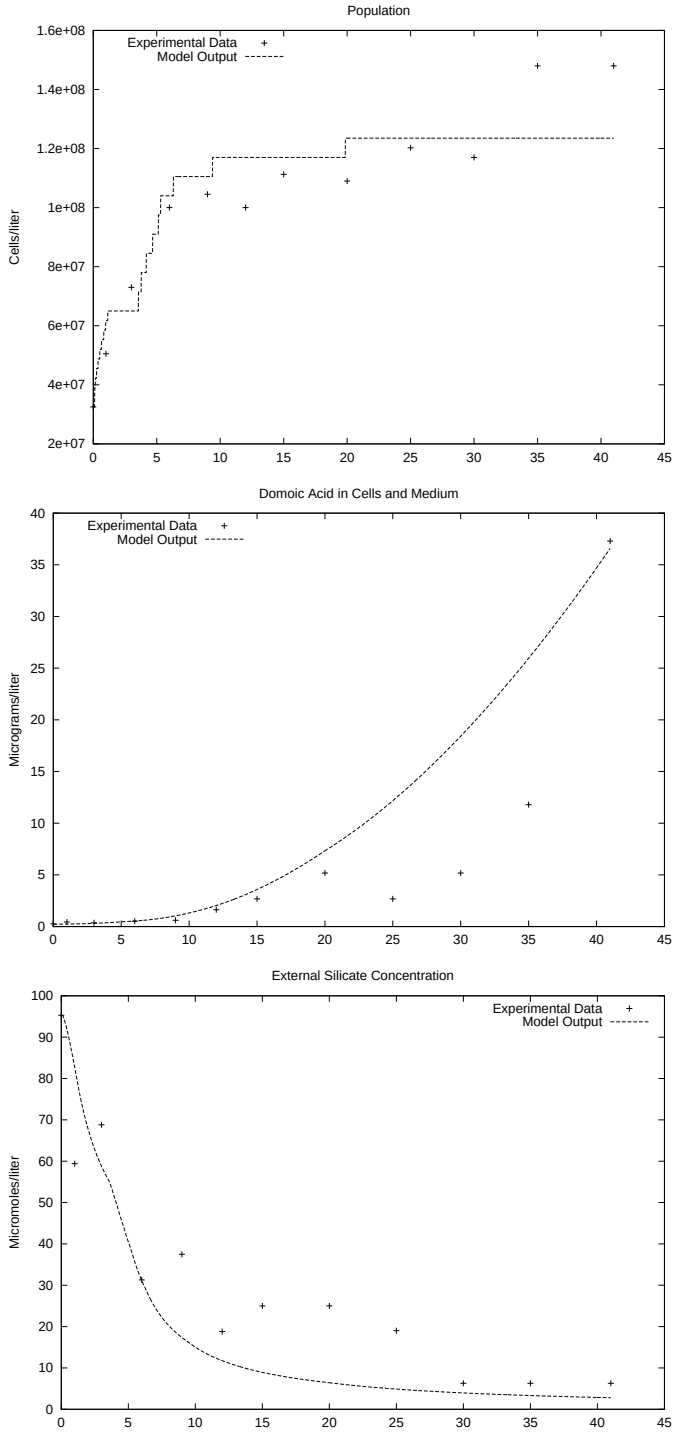

Figure A.11: Experimental data and model output for experiment A: Medium Si concentration

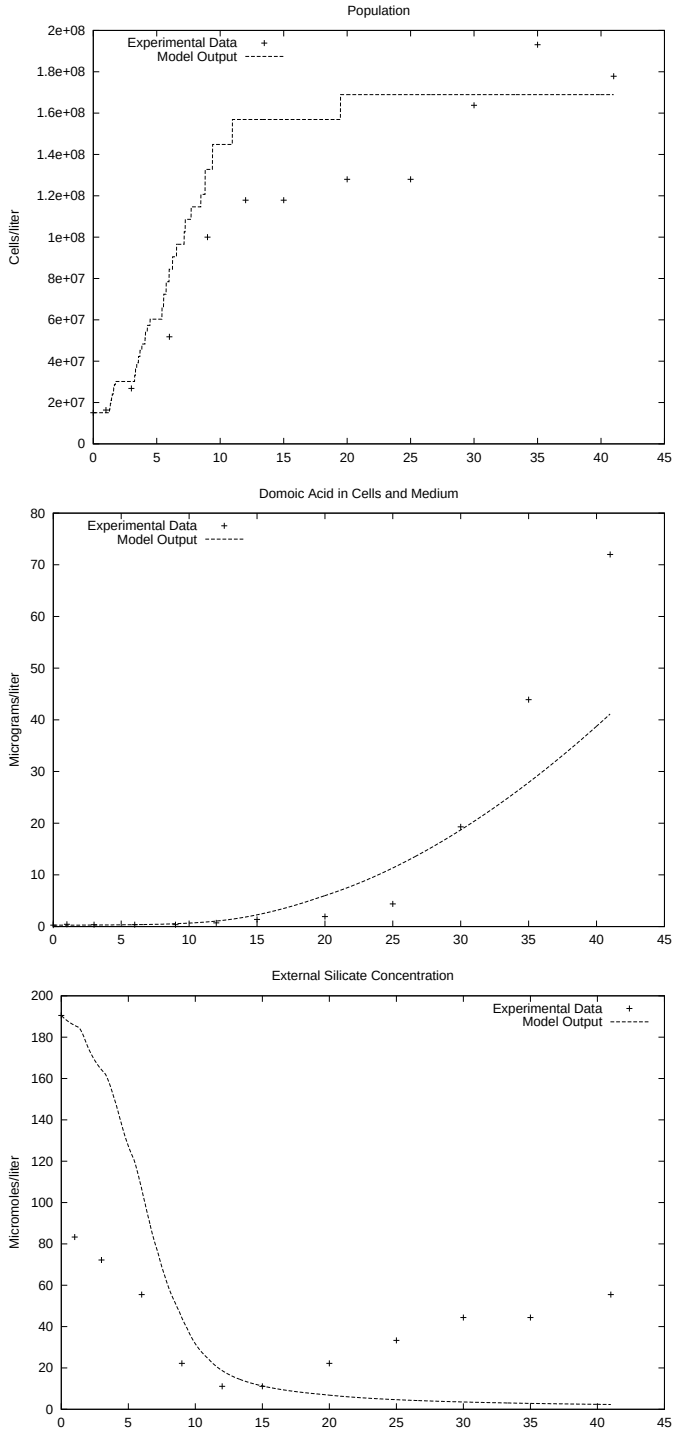

Figure A.12: Experimental data and model output for experiment B: High Si concentration

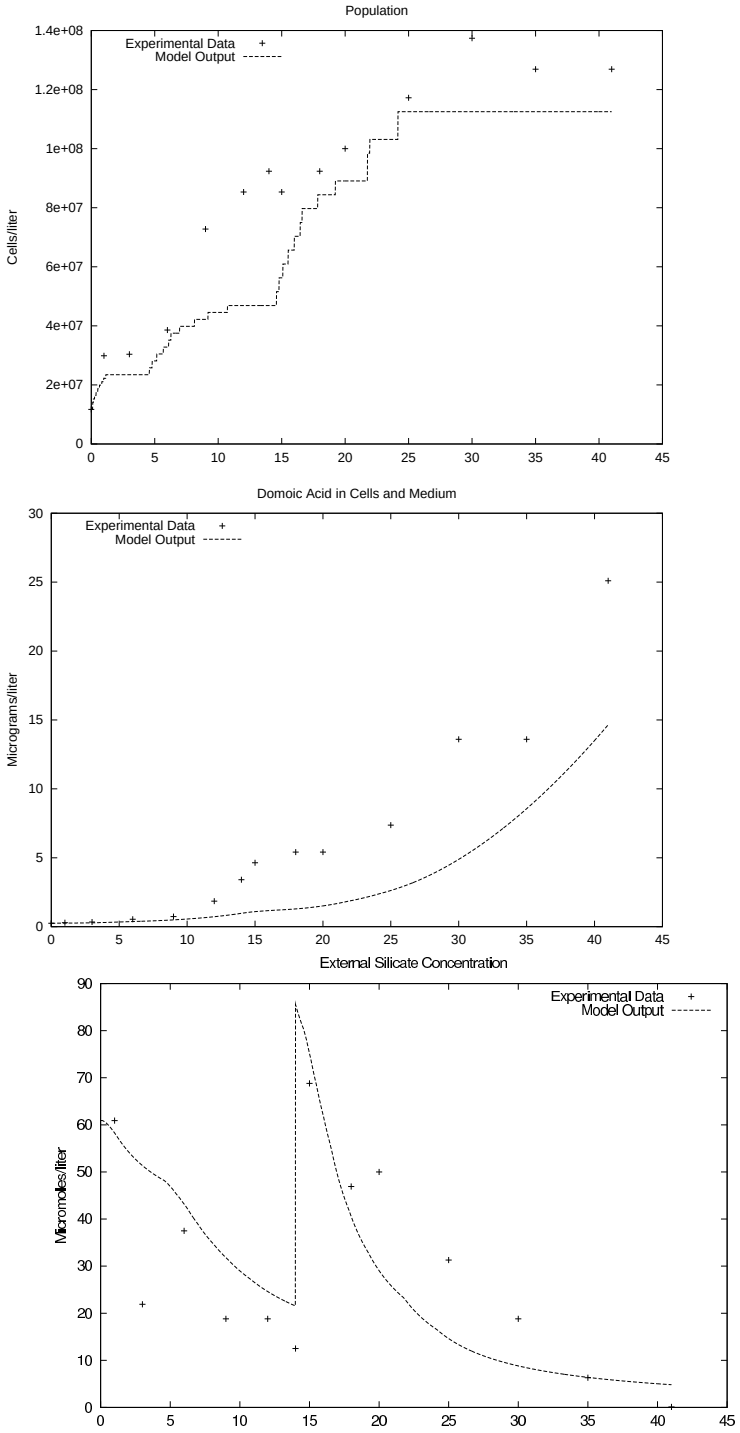

Figure A.13: Experimental data and model output for experiment C: Perturbed batch experiment. Si added on day 14.

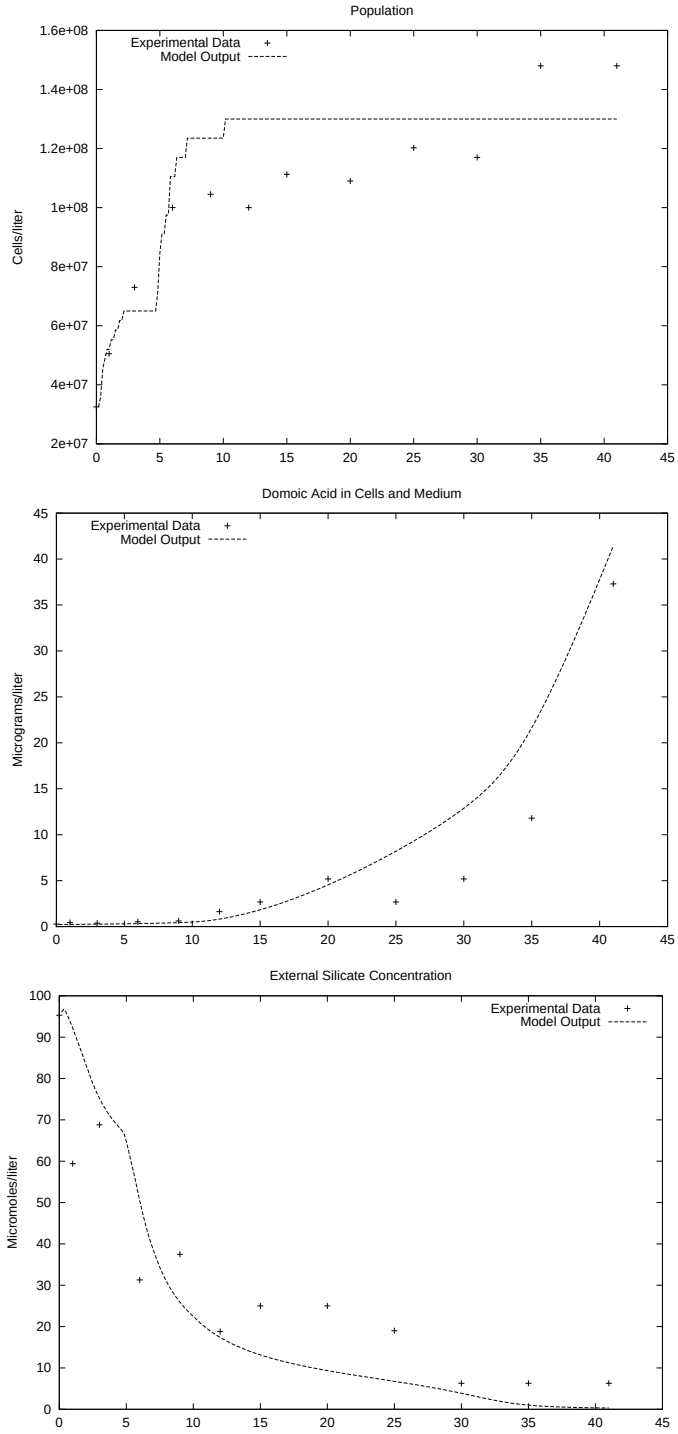

Figure A.14: Experimental data and model output for Experiment A: Low initial external Si concentration

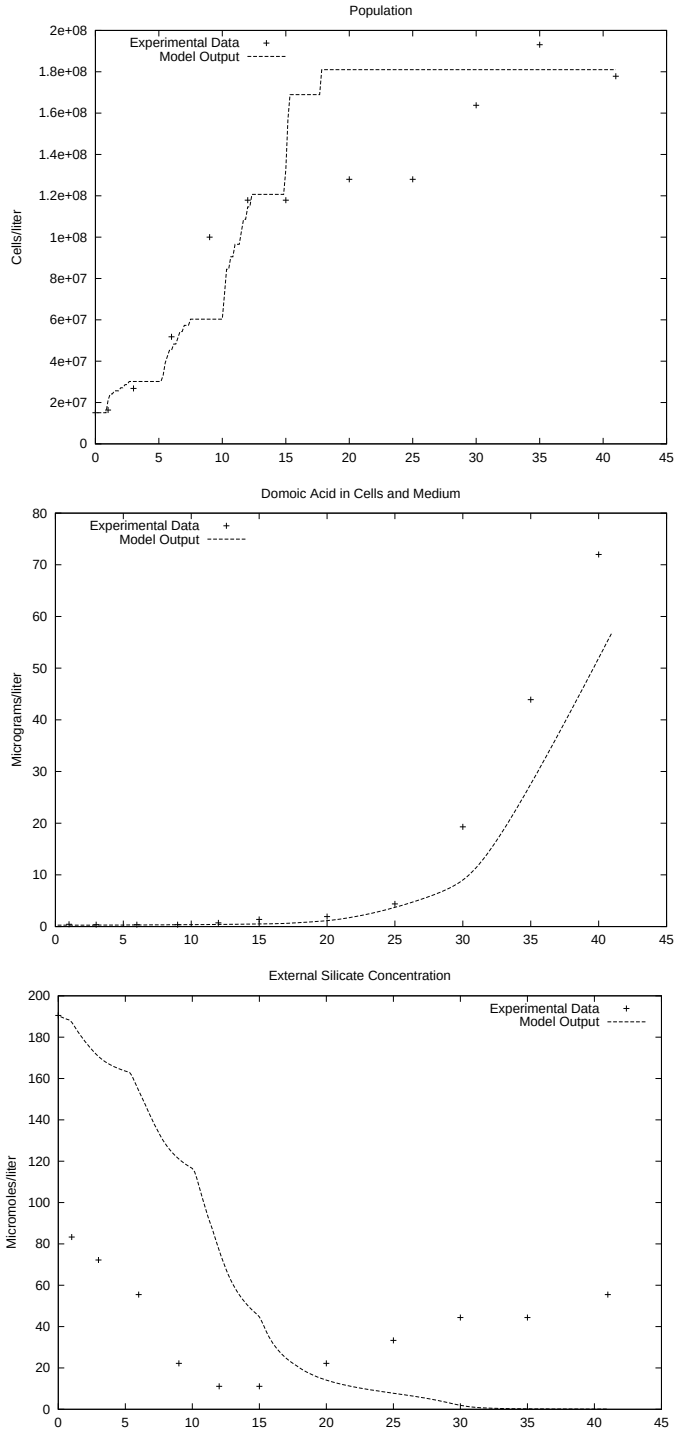

Figure A.15: Experimental data and model output for experiment B: High initial external SI concentration

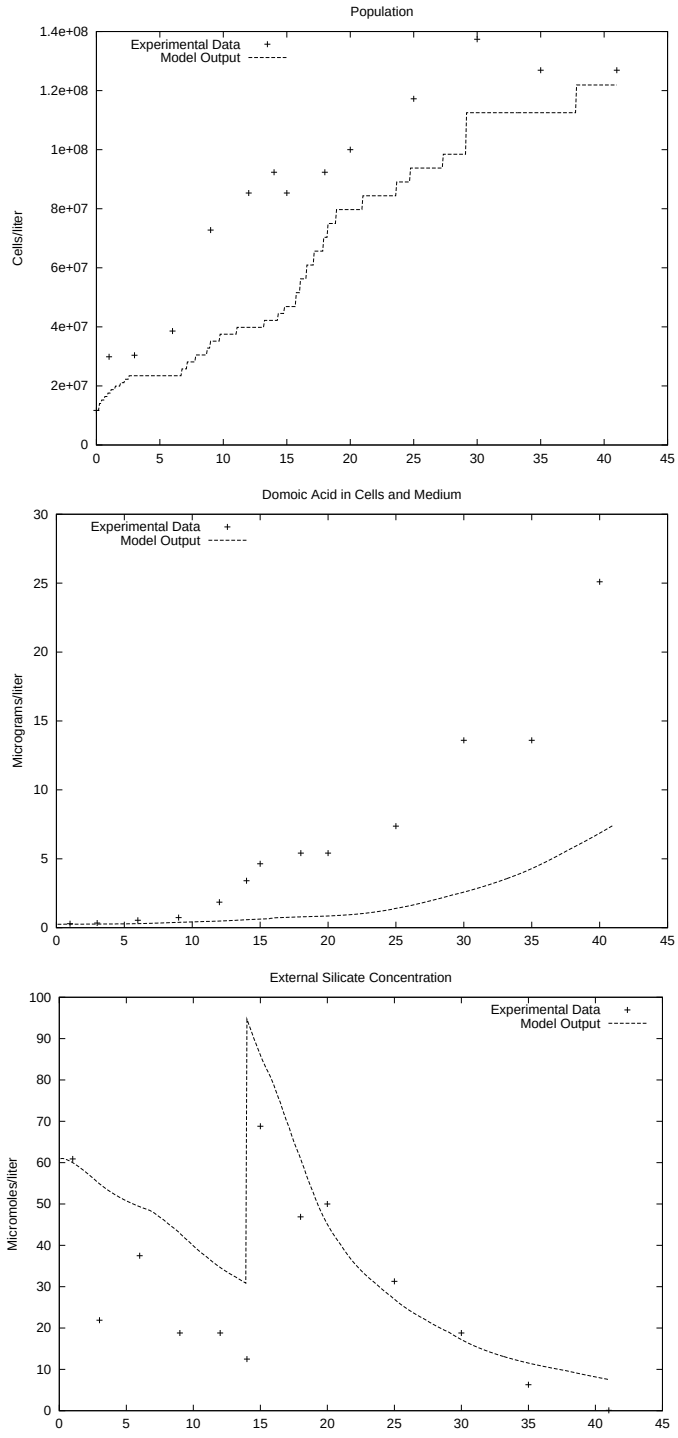

Figure A.16: Experimental data and model output for experiment C: Perturbed batch experiment. Si added on day 14

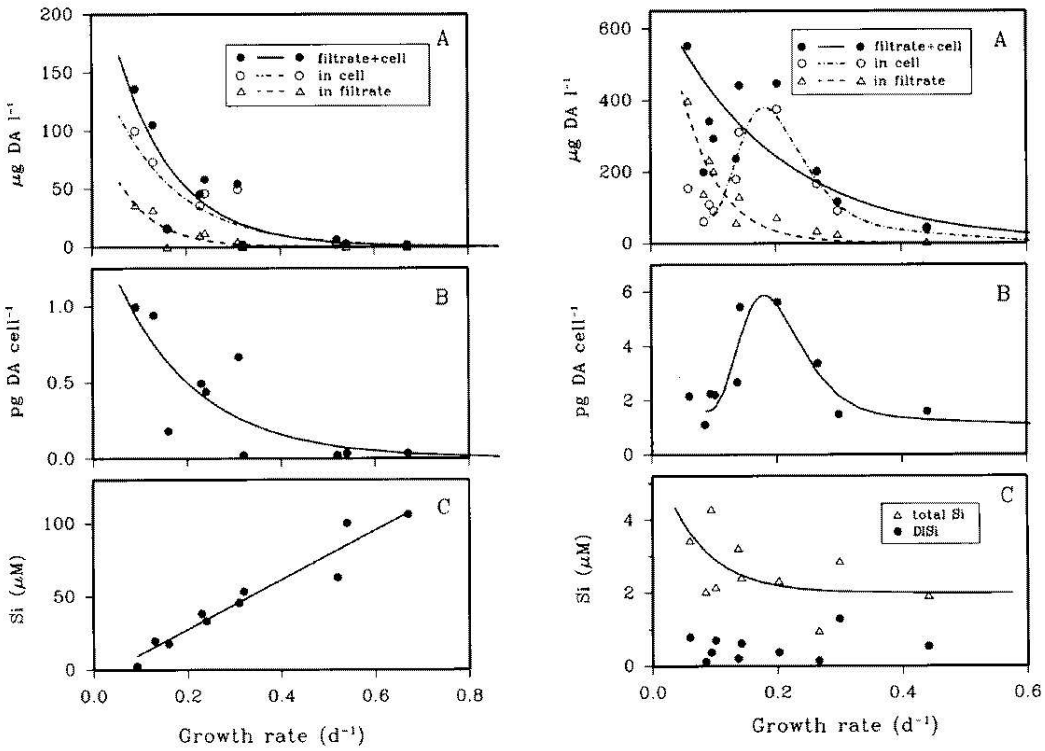

Figure A.17: Data from chemostat experiments 1 (left) and 2. Graph A shows total DA in the system, DA in the cells, and DA in the medium with respect to growth rate. Graph B shows internal cellular DA with respect to growth rate. Graph C shows external Si concentration with respect to growth rate. Recreated from Pan et al., [59].

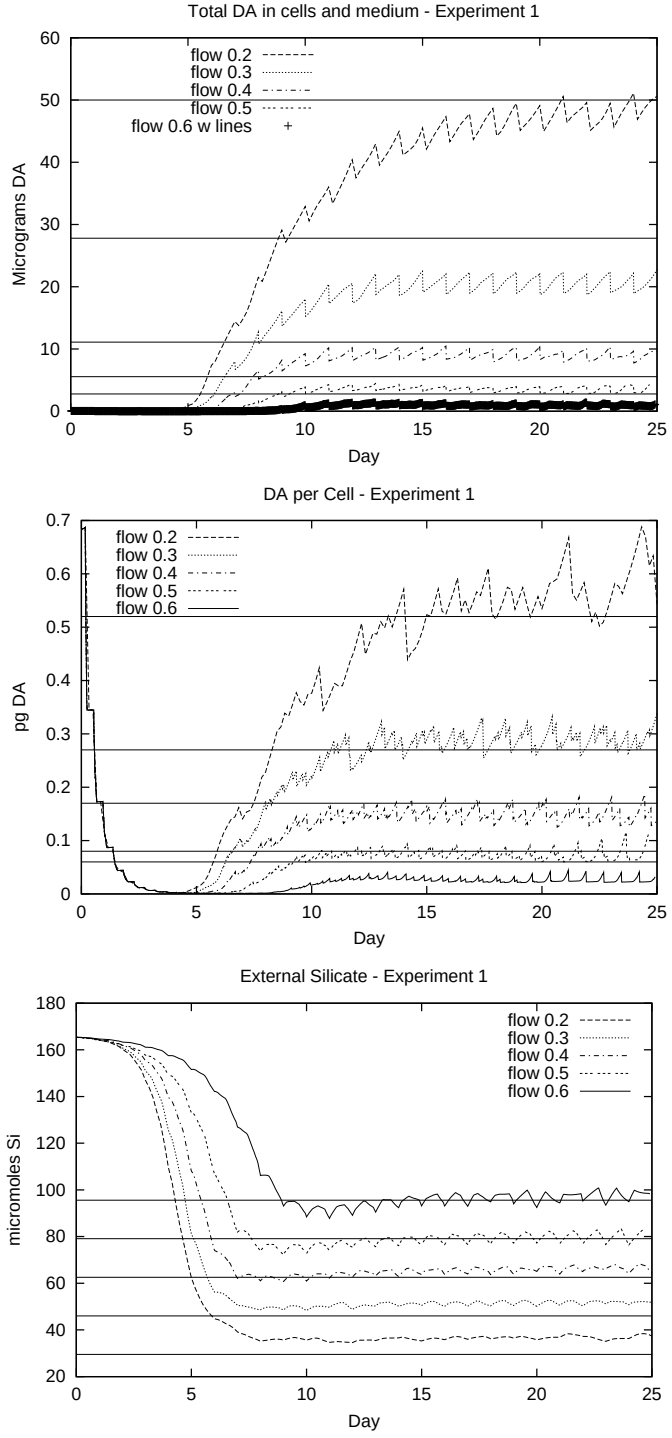

Figure A.18: Model results for chemostat Experiment 1, time series data. Solid lines show data. The model is within 24.7% of Si data. For flow rates 0.2-0.5d^{-1}, total DA and DA per cell are within 35.6% of the data and 16.7% of the data, respectively. For the 0.6d^{-1} flow rate, model output is within 0.035 pg of the data for DA/cell and 1.6 μg of the total DA.

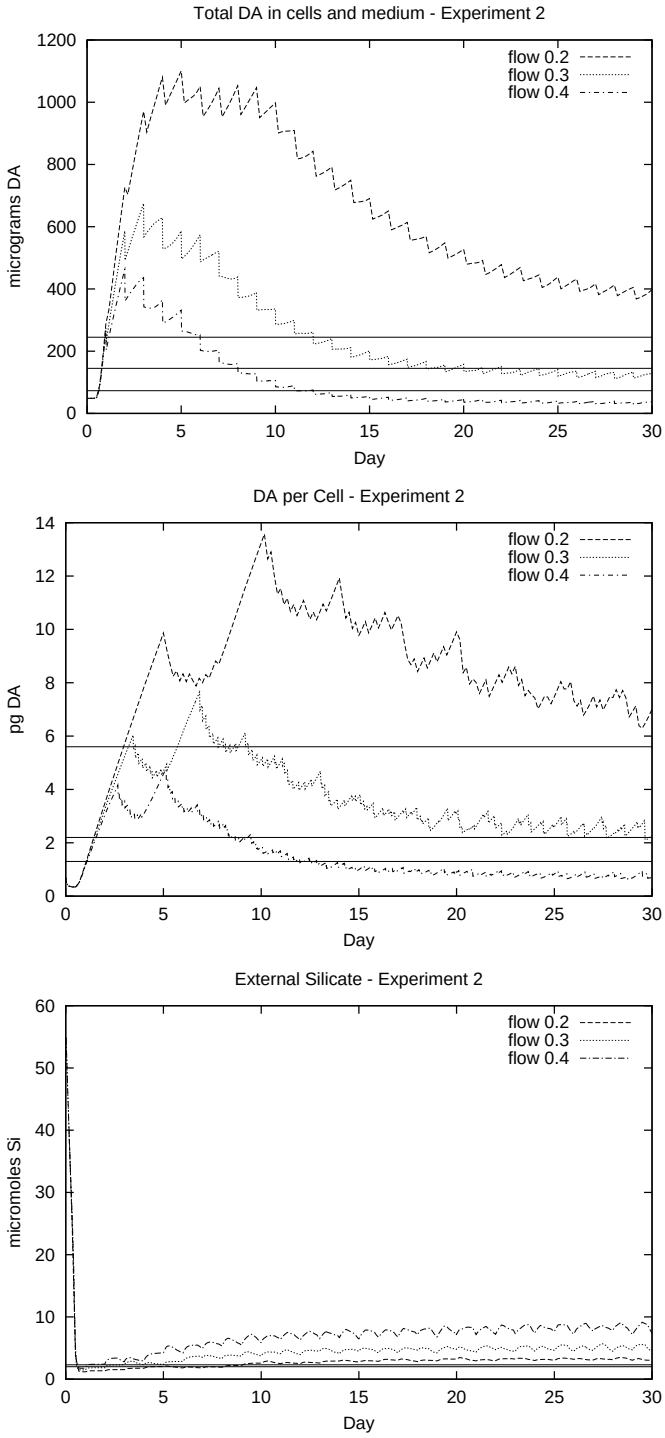

Figure A.19: Model results for chemostat Experiment 2, time series data. Solid lines show data. Total DA indicates an overestimation of the algae population by the model. DA/cell is at worst 2.5 pg from the actual data.

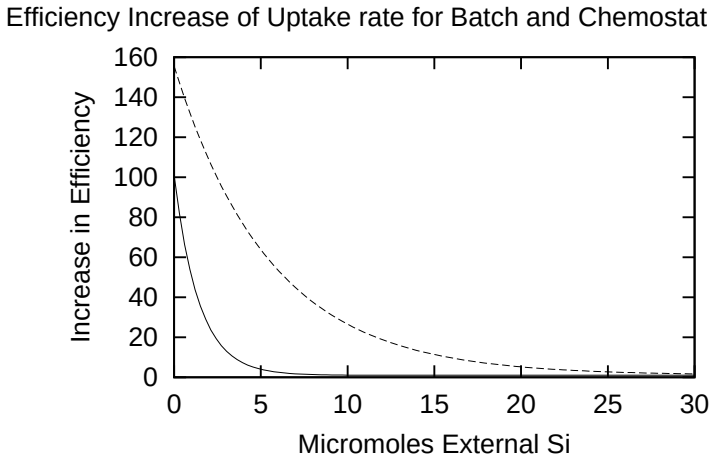

Figure A.20: Efficiency increase curves as a function of external Si for batch (solid line) and chemostat (dashed line) model parameter sets.

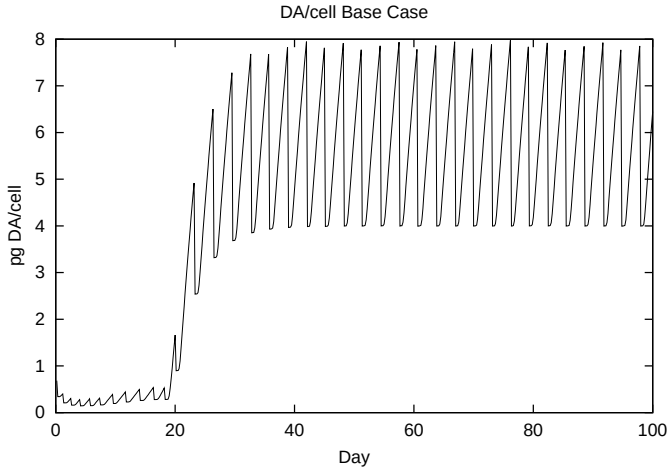

Figure A.21: DA/cell for chemostat Experiment 2 with flow rate 20% day^{-1}.

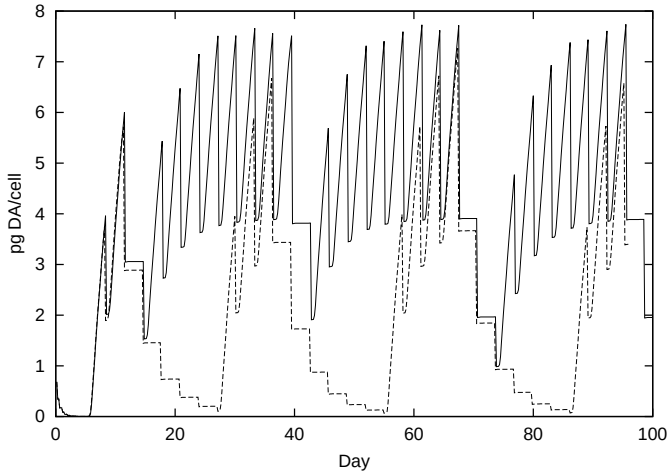

Figure A.22: DA/cell, increased Si. Solid line is 1405 μmol/L Si, dashed is 1465 μmol/L Si.

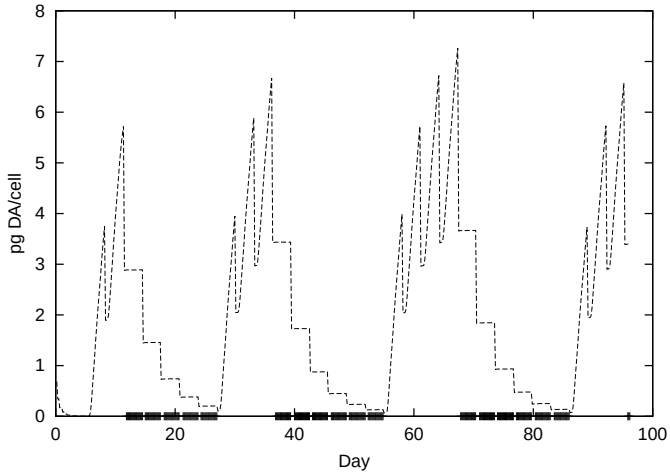

Figure A.23: DA/cell, external Si 1465 μmol/L. Sections of x axis in bold denote periods of N limitation.

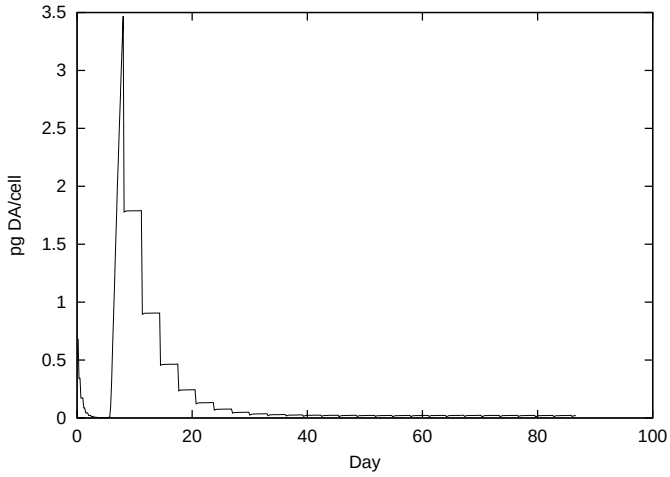

Figure A.24: DA/cell, external Si 1500 μmol. Production is low after an initial spike.

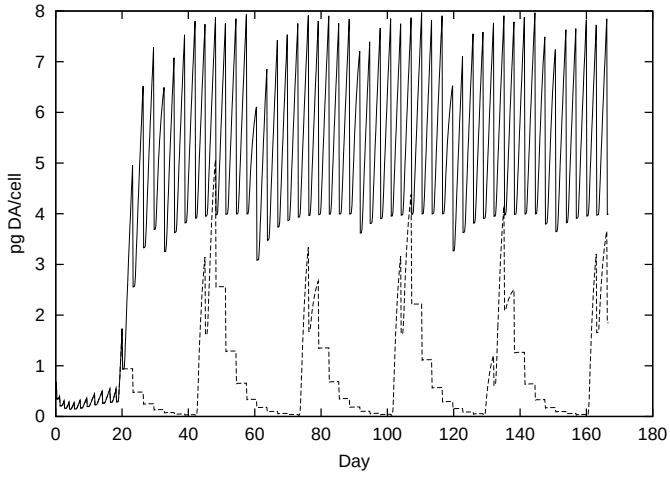

Figure A.25: DA/cell for flow rate 20%day^{-1}. Solid line is 65 μmol N/L , dashed is 61 μmol N/L.

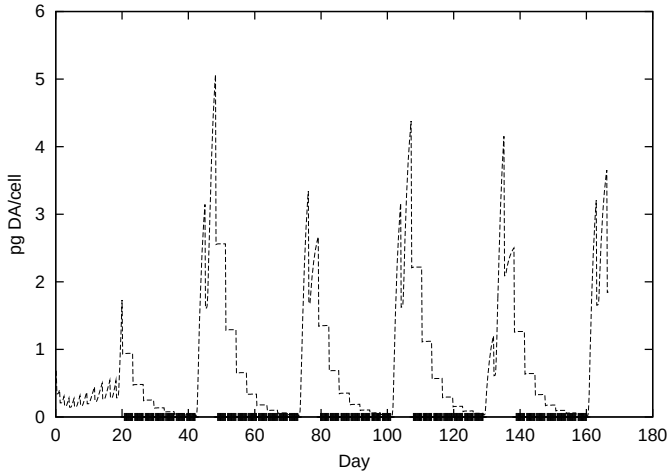

Figure A.26: DA/cell for flow rate 20%day^{-1}, external N 61 μmol/L. Sections of x axis in bold denote periods of N limitation.

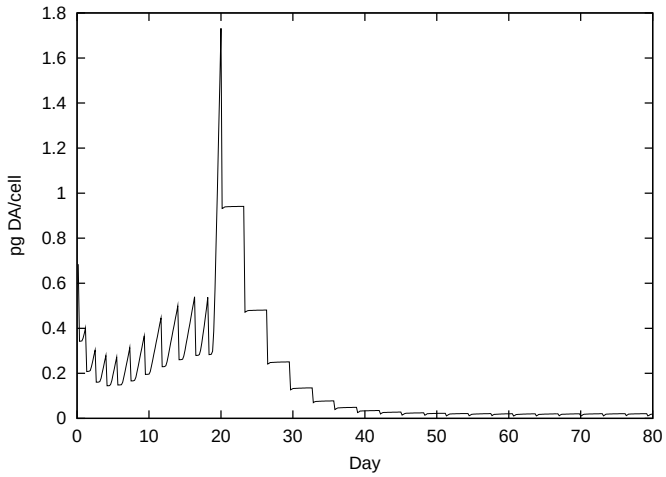

Figure A.27: DA/cell for flow rate 20%day^{-1}, external N 60 μmol. Production is low after an initial spike.

Appendix B

Tables

Table B.1: Some blooms of *Pseudo-nitzschia* species and their effects

Location	Date	Species	Consequences
Prince Edward Island, Canada	September, 2000	*P. Multiseries*	Closure of mollusc fishery [41]
Aveiro Lagoon, Portugal	October, November 1998	*P. australis*	None, previous closure for other toxins [31]
East coast of Scotland	May 1998	*Pseudo-nitzschia* spp	Scallop fishery closed [31]
Orkney Islands, Scotland	May-december 1998	*Pseudo-nitzschia* spp	Scallop fishery closed [31]
Shetland Islands, Scotland	May, June, August 1998	*Pseudo-nitzschia* spp	Fishery closed [31]
West Coast of Scotland	April-October 1998	*Pseudo-nitzschia* spp	Fishery closed [31]
Galicia, Spain	October, November, 1998	*Pseudonitzschia* spp	Fishery closed [31]
Andalucia, Spain	June, 1998	*Pseudo-nitzschia* spp	Shellfish grounds closed [31]
West Coast of Scotland	July 1999	*Pseudo-nitzschia* spp	Scallop fishery closed [47]
Morro Bay California	July 2000	*P. australis*	Bivalve, anchovy and sardine fisheries closed [76]
Oregon, USA	July 1998		All mussel and clam harvesting closed [15]
Washington State, USA	October, 1998		Razor clam harvest closed [34]
Central California, USA	August 2000		Sea Lion Mortality [52]
Washington and Oregon coasts, USA	October 1991 - May 1992	*Pseudonitzschia* spp	Commercial shellfish fishery closed [37]
Monterey Bay, California, USA	September 1991	*P. australis*	Pelican and cormorant deaths [30]
Prince Edward Island, Canada	Autumn 1987	*P. multiseries*	Human illness, death [2]

Table B.2: Model Variables

Variable	Description	Units
N_e	External nitrogen concentration	μmols/cm^3
P_e	External phosphorus concentration	μmols/cm^3
S_e	External silicon concentration	μmols/cm^3
DA_e	External DA concentration	μmols/cm^3
N_i	Internal nitrogen pool	μmols
P_i	Internal phosphorus pool	μmols
E	Internal ATP pool	μmols
SI_i	Internal silicon pool	μmols
m_{Pr}	Mass of protein	μmols
m_{Ps}	Mass of polysaccharide	μmols
m_{Lp}	Mass of lipid	μmols
m_{Fr}	Mass of frustule	μmols
m_{Da}	Domoic acid pool	μmols
SA	Surface Area	cm^2
V	Volume	cm^3
I	Irradiance	$[\mu\text{molm}^{-2}\text{s}^{-1}]^{-1}$
$\delta()$	Cell density	cells/liter
Z	Grazer density	#/m^3
T	Temperature	
$v(T)$	Transport velocity	μmols cm s^{-1}

Table B.3: Model Parameters

Name	Description	Units
	Uptake Parameters	
a	Cell wall thickness	cm
c_{ϕ_e}	proportionality constant for external substance ϕ	s/cm^3
n_{ϕ_e}	density of transport sites for external substance ϕ	cm^{-2}
c_{ϕ_i}	inhibition of internal concentration of ϕ on uptake rate	nd
	Temperature Dependence Parameters	
S	Rate constant	μmols cm s^{-1}
T_A	Arrhenius temperature	degrees Kelvin
T_1	Chosen reference temperature	degrees Kelvin
	Surface and Volume Parameters	
σ_{Ps}	Molecular density of a polysaccharide	μmols/cm^3
σ_{Lp}	Molecular density of a lipid	μmols/cm^3
σ_{Pr}	Molecular density of a protein	μmols/cm^3
	Photosynthesis Parameters	
P_{max}	Maximum photosynthetic rate	$\frac{\mu\text{molC}}{\mu\text{molCbiomass} \quad s}$
α	Initial slope of photosynthesis-irradiance curve	$\frac{\mu\text{molC}\mu\text{molm}^2\text{s}}{\mu\text{molCbiomass} \quad \text{s}}$
β	Photoinhibition index	$\frac{\mu\text{molC}\mu\text{molm}^2\text{s}}{\mu\text{molCbiomass} \quad \text{s}}$
	Anabolism and Catabolism Parameters	
C_{ϕ_i}	Wait time for one molecule of substance ϕ_i	s
k_{ϕ_i,ϕ_s}	Number of atoms of substance ϕ_i per one atom of carbon in substance ϕ_s	
I_{m,ϕ_s}	Building time for one molecule of substance ϕ_S	s

continued on next page

Table B.3 continued

Name	Description	Units
$k_{\phi_s,0}$	Maximum catabolic rate for substance ϕ_S	μmols/s
$k_{\phi_s,1}$	Catabolic constant	nd
$k_{\phi_s,2}$	Catabolic constant	nd
$k_{\phi_s,3}$	Catabolic constant	μmuls/s
m_{0,ϕ_s}	Maximum number of ϕ_s molecules fixed per time	
Energy Flux Parameters		
M_0	Maintenance cost	$s^{-1}\mu mol^{-1}$
j_C	Fraction of carbon pool respired per second	s^{-1}
Reproduction Parameters		
l	Proportion of biomass lost from smaller daughter cell	nd
$m_{Pr,Tr}$	Mass of protein which triggers gamete production	μmols
Grazer Parameters		
M_i	Maximum ingestion rate for grazer	s^{-1}
A_e	Assimilation efficiency of grazer	nd
κ	Half saturation constant for grazer feeding	cells/l
θ	Mortality rate for grazer	s^{-1}

Table B.4: Base model parameter values for sensitivity analysis. Parameters not referenced were taken from Miller [55]

Parameter	Description	Value
Uptake		
a	Cell wall thickness	5.000e-6 [54]
c_N	Proportionality constant for external N	5.100e4 [67, 11]
c_{OP}	Proportionality constant for external OP	1.700e2 [21]
c_{si}	Proportionality constant for external Si	12.40e7 [11]
$c_{N,i}$	Inhibition of uptake rate of N by internal pool concentration of N	1.000e-4
$c_{OP,i}$	Inhibition of uptake rate of OP by internal pool concentration of OP	9.500e-3
c_{Si_i}	Inhibition of uptake rate of Si by internal pool concentration of Si	1.000e-2
n_{N_e}	Density of transport sites for N uptake	9.000e5 [67, 11]
$n_{OP,e}$	Density of transport sites for OP uptake	1.100e2 [21]
$n_{Si,e}$	Density of transport sites for Si uptake	2.000e3 [11]
λ_0	Maximum increase in uptake efficiency for Si	0.000
ρ	Decrease in uptake efficiency per unit external Si	0.000
Temperature Dependence		
S	Rate constant	2.160e-10 [67]
T_A	Arrhenius temperature	8488 [67]

continued on next page

Table B.4 continued

Parameter	Description	Value
T_1	Chosen reference temperature	280.0 [67]
	Surface and Volume	
σ_{Ps}	Molecular density of a polysaccharide	2.600e-10
σ_{Lp}	Molecular density of a lipid	2.000e-10
σ_{Pr}	Molecular density of a protein	1.250e-10
	Photosynthesis	
P_{max}	Maximum photosynthetic rate	1.200e-2 [62]
α	Initial slope of photosynthesis-irradiance curve	5.000e-5 [62]
β	Photoinhibition index	6.000e-5 [62]
	Energy Fluxes	
M_0	Maintenance cost	2.200e-18
j_C	Fraction of carbon pool respired per second	1.000e-4
	Anabolism and Catabolism	
C_{C_i}	Wait time for one molecule of C	2.000e-6
$C_{N,i}$	Wait time for one molecule of N	2.000e-6
C_{P_i}	Wait time for one molecule of P	2.000e-6
C_{E_i}	Wait time for one molecule of ATP	16.50e-6
C_{Si_i}	Wait time for one molecule of Si	2.000e-6
$k_{N,Pr}$	Number of atoms of N per one atom of C in protein	1.800e-1 [43]
$k_{N,Ps}$	Number of atoms of N per one atom of C in polysaccharide	0.000 [13]

continued on next page

Table B.4 continued

Parameter	Description	Value
$k_{N,Lp}$	Number of atoms of N per one atom of C in lipid	0.000 [63, 56]
$k_{P,Pr}$	Number of atoms of P per one atom of C in protein	0.000 [43]
$k_{P,Ps}$	Number of atoms of P per one atom of C in polysaccharide	0.000 [13]
$k_{N,Lp}$	Number of atoms of P per one atom of C in lipid	5.000e-2 [63, 56]
$k_{E,Pr}$	Number of atoms of ATP per one atom of C in protein	2.500
$k_{E,Ps}$	Number of atoms of ATP per one atom of C in polysaccharide	1.000[1]
$k_{E,Lp}$	Number of atoms of ATP per one atom of C in lipid	0.500 [16]
$k_{E,Fr}$	Number of atoms of ATP per one atom of Si in frustule	6.000e-4
$I_{m,Pr}$	Building time for one molecule of protein	1.000
$I_{m,Ps}$	Building time for one molecule of polysaccharide	1.000
$I_{m,Lp}$	Building time for one molecule of lipid	1.000
$I_{m,Fr}$	Building time for one molecule of frustule	1.000
$I_{m,DA}$	Building time for one molecule of DA	1.000
$k_{Ps,0}$	Maximum catabolic rate for polysaccharides	2.300e-10
$k_{Lp,0}$	Maximum catabolic rate for lipids	2.300e-9

continued on next page

Table B.4 continued

Parameter	Description	Value
$k_{Ps,1}$	Catabolic constant	2.000e-1
$k_{Lp,1}$	Catabolic constant	2.000e-1
$k_{Ps,2}$	Catabolic constant	1.000e9
$k_{Lp,2}$	Catabolic constant	1.000e9
$k_{Ps,3}$	Catabolic constant	1.000e-10
$k_{Lp,3}$	Catabolic constant	1.000e-6
$m_{0,Pr}$	Maximum number of protein molecules fixed per time	1.800e-6
$m_{0,Ps}$	Maximum number of polysaccharide molecules fixed per time	6.400e-7
$m_{0,Lp}$	Maximum number of lipid molecules fixed per time	3.500e-7
$m_{0,Fr}$	Maximum number of frustule molecules fixed per time	7.500e-6
$m_{0,DA}$	Maximum number of DA molecules fixed per time	1.000e-10

Table B.5: ANOVA table for 5-variable factorial design: Population data

Variable	Sum Sq.	d.f.	Mean Sq.	F	p
C_E	246.505	4	61.6262	4333.22	0
β	2.993	4	0.7483	52.62	0
P_{max}	5.78	4	1.4449	101.6	0
T_1	20.26	4	5.0651	356.15	0
$k_{E,Pr}$	1.525	4	0.3813	26.81	0
C_E with β	7.476	16	0.4672	32.85	0
C_E with P_{max}	12.023	16	0.7514	52.84	0
C_E with T_1	41.928	16	2.6205	184.26	0
C_E with $k_{E,Pr}$	1.164	16	0.0728	5.12	0
β with P_{max}	1.188	16	0.0743	5.22	0
β with T_1	0.32	16	0.02	1.4	0.1297
β with $k_{E,Pr}$	0.07	16	0.0043	0.31	0.9962
P_{max} with T_1	0.5	16	0.0312	2.2	0.004
P_{max} with $k_{E,Pr}$	0.109	16	0.0068	0.48	0.9578
T_1 with $k_{E,Pr}$	3.757	16	0.2348	16.51	0
Error	41.869	2944	0.0142		
Total	387.467	3124			

Table B.6: Summary of F and p values for ANOVA tests for 5-variable factorial experiment: Population data

Variable	F	p	F	p	F	p	F	p
C_E	4333.22	0			352.44	0	1193.75	0
β	52.62	0	6.42	0	65.92	0	16.08	0
P_{max}	101.6	0	12.4	0	102.01	0	31.63	0
T_1	365.15	0	43.47	0	2998.65	0	560.25	0
$k_{E,Pr}$	26.81	0	3.27	0.011	37.06	0	13.19	0
C_E with β	32.85	0			18.93	0	14.56	0
C_E with P_{max}	52.84	0			19.28	0	28.28	0
C_E with T_1	184.26	0			8.55	0	74.98	0
C_E with $k_{E,Pr}$	5.12	0			6.99	0	5.01	0
β with P_{max}	5.22	0	0.64	0.8557	45.24	0	1.66	0.0938
β with T_1	1.40	0.1297	0.17	0.9999	4.5	0	3.79	0.0001
β with $k_{E,Pr}$	0.31	0.9962	0.04	1	3.65	0	0.24	0.9882
P_{max} with T_1	2.2	0.004	0.27	0.9983	11.78	0	7.21	0
P_{max} with $k_{E,Pr}$	0.48	0.9578	.06	1	7.63	0	0.35	0.9583
T_1 with $k_{E,Pr}$	16.51	0	2.02	0.0096	20.91	0	6.87	0

Table B.7: ANOVA table for 5-variable factorial experiment: DA data

Variable	Sum Sq.	d.f.	Mean Sq.	F	p
C_E	28.041	4	7.0103	162.49	0
β	6.775	4	1.6937	39.26	0
P_{max}	10.916	4	2.729	63.25	0
T_1	107.902	4	26.9755	625.26	0
$k_{E,Pr}$	34.915	4	8.7288	202.32	0
C_E with β	3.729	16	0.2331	5.4	0
C_E with P_{max}	8.35	16	0.5219	12.1	0
C_E with T_1	38.149	16	2.3843	55.27	0
C_E with $k_{E,Pr}$	7.363	16	0.4602	10.67	0
β with P_{max}	5.526	16	0.3454	8.01	0
β with T_1	25.76	16	1.61	37.32	0
β with $k_{E,Pr}$	8.371	16	0.5232	12.13	0
P_{max} with T_1	45.385	16	2.8365	65.75	0
P_{max} with $k_{E,Pr}$	13.757	16	0.8598	19.93	0
T_1 with $k_{E,Pr}$	44.304	16	2.769	64.18	0
Error	127.013	2944	0.0431		
Total	516.257	3124			

Table B.8: ANOVA table for 5-variable factorial experiment: External Si data

Variable	Sum Sq.	d.f.	Mean Sq.	F	p
C_E	134695.5	4	33673.9	4296.38	0
β	2111.7	4	527.9	67.36	0
P_{max}	4098	4	1024.5	130.71	0
T_1	112117.1	4	28029.3	3576.2	0
$k_{E,Pr}$	1288.1	4	322	41.09	0
C_E with β	4491.2	16	280.7	35.81	0
C_E with P_{max}	8801.8	16	550.1	70.19	0
C_E with T_1	28687.6	16	1793	228.76	0
C_E with $k_{E,Pr}$	1048.1	16	65.5	8.36	0
β with P_{max}	384.6	16	24	3.07	0
β with T_1	346	16	21.6	2.76	0.0002
β with $k_{E,Pr}$	77.5	16	4.8	0.62	0.8721
P_{max} with T_1	677.8	16	42.4	5.41	0
P_{max} with $k_{E,Pr}$	154.7	16	9.7	1.23	0.2331
T_1 with $k_{E,Pr}$	3023	16	188.9	24.11	0
Error	23074.3	2944	7.8		
Total	325076.9	3124			

Table B.9: Summary of F and p values for ANOVA tests on 5-variable factorial experiment: External Si data

Variable	F	p	F	p	F	p	F	p
C_E	4296.38	0			93.08	0	966.8	0
β	67.36	0	7.92	0	45.57	0	18.91	0
P_{max}	130.71	0	15.37	0	60.99	0	43.51	0
T_1	3576.2	0	420.44	0	85051.67	0	3020.52	0
$k_{E,Pr}$	41.09	0	4.83	0.0007	120.18	0	19.96	0
C_E with β	35.81	0			7.22	0	15.49	0
C_E with P_{max}	70.19	0			9.48	0	37.22	0
C_E with T_1	228.76	0			38.81	0	85.59	0
C_E with $k_{E,Pr}$	8.36	0			13.58	0	9.26	0
β with P_{max}	3.07	0	0.36	0.9903	8.97	0	1.41	0.1796
β with T_1	2.76	0.0002	0.32	0.9947	2.6	0.0005	3.19	0.0008
β with $k_{E,Pr}$	0.62	0.8721	0.07	1	0.55	0.9205	0.18	0.9963
P_{max} with T_1	5.41	0	0.64	0.8574	2.61	0.0005	8.13	0
P_{max} with $k_{E,Pr}$	1.23	0.2331	0.15	1	0.34	0.9933	0.15	0.9979
T_1 with $k_{E,Pr}$	24.11	0	2.83	0.0001	20.4	0	10.66	0

Table B.10: ANOVA table for 8-variable factorial experiment: Population data

Variable	Sum Sq.	d.f.	Mean Sq.	F	p
C_E	95.723	2	47.8616	3068.82	0
β	3.756	2	1.8782	120.42	0
P_{max}	3.685	2	1.8426	118.15	0
T_1	21.02	2	10.5099	673.88	0
$k_{E,Pr}$	0.008	2	0.0042	0.27	0.7618
$M_{0,Fr}$	67.255	2	33.6277	2156.16	0
C_{Si_i}	1.389	2	0.6945	44.53	0
$n_S i$	0.05	2	0.0252	1.62	0.1985
C_E with β	4.543	4	1.1359	72.83	0
C_E with P_{max}	11.128	4	2.782	178.38	0
C_E with T_1	13.159	4	3.2897	210.93	0
C_E with $k_{E,Pr}$	0.402	4	0.1004	6.44	0
C_E with $M_{0,Fr}$	98.862	4	24.7154	1584.72	0
C_E with C_{Si_i}	0.019	4	0.0047	0.3	0.8783
C_E with $n_S i$	0.111	4	0.0279	1.79	0.1285
β with P_{max}	3.642	4	0.9105	58.38	0
β with T_1	0.174	4	0.0435	2.79	0.0249
β with $k_{E,Pr}$	0.121	4	0.0302	1.93	0.1017
β with $M_{0,Fr}$	9.402	4	2.3505	150.71	0
β with C_{Si_i}	0.205	4	0.0512	3.29	0.0107
β with $n_S i$	0.01	4	0.0025	0.16	0.9571
P_{max} with T_1	0.45	4	0.1124	7.21	0
P_{max} with $k_{E,Pr}$	0.842	4	0.2104	13.49	0
P_{max} with $M_{0,Fr}$	1.392	4	0.3479	22.31	0
P_{max} with C_{Si_i}	0.551	4	0.1378	8.84	0
P_{max} with $n_S i$	0.024	4	0.0061	0.39	0.8166
T_1 with $k_{E,Pr}$	0.051	4	0.0126	0.81	0.5187
T_1 with $M_{0,Fr}$	2.087	4	0.5217	33.45	0
T_1 with C_{Si_i}	3.816	4	0.9541	61.17	0
T_1 with $n_S i$	0.066	4	0.0164	1.05	0.3797
$k_{E,Pr}$ with $M_{0,Fr}$	0.02	4	0.0049	0.32	0.8671
$k_{E,Pr}$ with C_{Si_i}	0.074	4	0.0184	1.18	0.3169
$k_{E,Pr}$ with $n_S i$	0.001	4	0.0001	0.01	0.9999
$M_{0,Fr}$ with C_{Si_i}	0.982	4	0.2455	15.74	0
$M_{0,Fr}$ with $n_S i$	0.025	4	0.0062	0.4	0.8107
C_{Si_i} with $n_S i$	0.011	4	0.0029	0.18	0.9466
Error	100.299	6431	0.0156		
Total	445.345	6559			

Table B.11: Summary of F and p values for ANOVA tests on 8-variable factorial experiment: Population data

Variable	F	p	F	p	F	p	F	p
C_E	3068.82	0			39.95	0	18.71	0
β	120.42	0	37.46	0	105.9	0	79.28	0
P_{max}	118.15	0	36.75	0	254.17	0	196.97	0
T_1	673.88	0	209.36	0	18495.63	0	21015.32	0
$k_{E,Pr}$	0.27	0.7618	0.08	0.9188	49.69	0	73.38	0
$M_{0,Fr}$	2156.16	0	669.93	0	554.97	0	564.99	0
C_{Si_i}	44.53	0	13.86	0	522.27	0	607.9	0
$n_S i$	1.62	0.1985	0.5	0.6074	1.75	0.1731	0.11	0.8971
C_E with β	72.83	0			4.83	0.0007	0.16	0.8537
C_E with P_{max}	178.38	0			5.97	0.0001	2.95	0.0523
C_E with T_1	210.93	0			35.72	0	39.74	0
C_E with $k_{E,Pr}$	6.44	0			3.25	0.0114	4.1	0.0167
C_E with $M_{0,Fr}$	1584.72	0			25.24	0	7.43	0.0006
C_E with C_{Si_i}	0.3	0.8783			3.92	0.0035	7.38	0.0006
C_E with $n_S i$	1.79	0.1285			2.01	0.0899	0.33	0.7194
β with P_{max}	58.38	0	18.14	0	347.36	0	333.77	0
β with T_1	2.79	0.0249	0.87	0.4832	43.95	0	54.91	0
β with $k_{E,Pr}$	1.93	0.1017	0.6	0.661	54.93	0	52.19	0
β with $M_{0,Fr}$	150.71	0	46.81	0	95.68	0	58.07	0
β with C_{Si_i}	3.29	0.0107	1.03	0.3922	48.96	0	55.46	0
β with $n_S i$	0.16	0.9571	0.05	0.9954	1.53	0.1899	0.18	0.9501
P_{max} with T_1	7.21	0	2.24	0.0621	125	0	119.42	0
P_{max} with $k_{E,Pr}$	13.49	0	4.18	0.0022	139.44	0	149.44	0
P_{max} with $M_{0,Fr}$	22.31	0	6.92	0	115.06	0	100.43	0
P_{max} with C_{Si_i}	8.84	0	2.74	0.0272	100.41	0	95.74	0
P_{max} with $n_S i$	0.39	0.8166	0.12	0.9744	3.07	0.0156	0.93	0.4447
T_1 with $k_{E,Pr}$	0.81	0.5187	0.25	0.9075	45.24	0	56.9	0
T_1 with $M_{0,Fr}$	33.45	0	10.39	0	455.94	0	627.01	0
T_1 with C_{Si_i}	61.17	0	19	0	709.52	0	564.72	0
T_1 with $n_S i$	1.05	0.3797	0.33	0.8593	1.07	0.3672	1.89	0.109
$k_{E,Pr}$ with $M_{0,Fr}$	0.32	0.8671	0.1	0.983	17.74	0	27.03	0
$k_{E,Pr}$ with C_{Si_i}	1.18	0.3169	0.37	0.8299	22.21	0	28.41	0
$k_{E,Pr}$ with $n_S i$	0.01	0.9999	0	1	1.67	0.1533	1.86	0.1143
$M_{0,Fr}$ with C_{Si_i}	15.74	0	4.88	0.006	182.27	0	228.01	0
$M_{0,Fr}$ with $n_S i$	0.4	0.8107	0.12	0.9736	0.14	0.9694	1.64	0.1622
C_{Si_i} with $n_S i$	0.18	0.9466	0.06	0.9936	1.67	0.1533	1.75	0.1358

Table B.12: ANOVA table for 8-variable factorial experiment: DA data

Variable	Sum Sq.	d.f.	Mean Sq.	F	p
C_E	26.74	2	13.368	597.34	0
β	18.71	2	9.353	417.92	0
P_{max}	14.46	2	7.23	323.07	0
T_1	532.03	2	266.017	11887.01	0
$k_{E,Pr}$	24.88	2	12.438	555.79	0
$M_{0,Fr}$	9.07	2	4.537	202.76	0
C_{Si_i}	0.01	2	0.007	0.29	0.7476
$n_S i$	0.03	2	0.016	0.73	0.4827
C_E with β	0.32	4	0.08	3.58	0.0063
C_E with P_{max}	7.71	4	1.926	86.08	0
C_E with T_1	16.47	4	4.117	183.98	0
C_E with $k_{E,Pr}$	0.76	4	0.189	8.46	0
C_E with $M_{0,Fr}$	18.48	4	4.62	206.46	0
C_E with C_{Si_i}	0.03	4	0.007	0.31	0.8686
C_E with $n_S i$	0.02	4	0.006	0.25	0.912
β with P_{max}	5.09	4	1.273	56.88	0
β with T_1	32.05	4	8.012	358.01	0
β with $k_{E,Pr}$	4.5	4	1.125	50.28	0
β with $M_{0,Fr}$	3.79	4	0.948	42.37	0
β with C_{Si_i}	0	4	0	0.02	0.9991
β with $n_S i$	0	4	0.001	0.03	0.9986
P_{max} with T_1	102.04	4	25.51	1139.92	0
P_{max} with $k_{E,Pr}$	10.3	4	2.574	115.03	0
P_{max} with $M_{0,Fr}$	5.76	4	1.44	64.35	0
P_{max} with C_{Si_i}	0.01	4	0.001	0.06	0.9942
P_{max} with $n_S i$	0.01	4	0.002	0.08	0.9896
T_1 with $k_{E,Pr}$	57.2	4	14.3	639.02	0
T_1 with $M_{0,Fr}$	16.91	4	4.227	188.9	0
T_1 with C_{Si_i}	0.26	4	0.065	2.92	0.02
T_1 with $n_S i$	0.34	4	0.084	3.77	0.0045
$k_{E,Pr}$ with $M_{0,Fr}$	0.35	4	0.088	3.94	0.0034
$k_{E,Pr}$ with C_{Si_i}	0.12	4	0.029	1.31	0.2649
$k_{E,Pr}$ with $n_S i$	0	4	0.001	0.03	0.9984
$M_{0,Fr}$ with C_{Si_i}	0.01	4	0.004	0.17	0.9557
$M_{0,Fr}$ with $n_S i$	0.01	4	0.002	0.1	0.9839
C_{Si_i} with $n_S i$	0	4	0	0.01	0.9996
Error	143.92	6431	0.022		
Total	1052.35	6559			

Table B.13: ANOVA table for 8-variable factorial experiment: External Silicon data

Variable	Sum Sq.	d.f.	Mean Sq.	F	p
C_E	46759.9	2	23380	3316.4	0
β	1172.3	2	586.2	83.15	0
P_{max}	5298.7	2	2649.3	375.8	0
T_1	77.1	2	38.5	5.46	0.0043
$k_{E,Pr}$	322.9	2	161.5	22.9	0
$M_{0,Fr}$	25016.4	2	12508.2	1774.26	0
C_{Si_i}	21.8	2	10.9	1.54	0.2138
$n_S i$	2	2	1	0.14	0.8657
C_E with β	2724.3	4	681.1	96.61	0
C_E with P_{max}	9075.4	4	2268.8	321.83	0
C_E with T_1	1986.1	4	496.5	70.43	0
C_E with $k_{E,Pr}$	366.7	4	91.7	13	0
C_E with $M_{0,Fr}$	50587.6	4	12646.9	1793.94	0
C_E with C_{Si_i}	63.9	4	16	2.27	0.0596
C_E with $n_S i$	48.6	4	12.2	1.72	0.1415
β with P_{max}	2426.9	4	606.7	86.06	0
β with T_1	49.1	4	12.3	1.74	0.1375
β with $k_{E,Pr}$	53.2	4	13.3	1.89	0.1097
β with $M_{0,Fr}$	4021.3	4	1005.3	142.6	0
β with C_{Si_i}	1.5	4	0.4	0.05	0.9946
β with $n_S i$	5.2	4	1.3	0.18	0.9474
P_{max} with T_1	376.1	4	94	13.34	0
P_{max} with $k_{E,Pr}$	72.5	4	18.1	2.57	0.0361
P_{max} with $M_{0,Fr}$	3274.2	4	818.5	116.11	0
P_{max} with C_{Si_i}	6	4	1.5	0.21	0.9324
P_{max} with $n_S i$	14.5	4	3.6	0.51	0.725
T_1 with $k_{E,Pr}$	476.7	4	119.2	16.9	0
T_1 with $M_{0,Fr}$	1032.3	4	258.1	36.61	0
T_1 with C_{Si_i}	29	4	7.3	1.03	0.3904
T_1 with $n_S i$	0.5	4	0.1	0.02	0.9995
$k_{E,Pr}$ with $M_{0,Fr}$	117.2	4	29.3	4.16	0.0023
$k_{E,Pr}$ with C_{Si_i}	4.8	4	1.2	0.17	0.9532
$k_{E,Pr}$ with $n_S i$	0.4	4	0.1	0.01	0.9996
$M_{0,Fr}$ with C_{Si_i}	45.9	4	11.5	1.63	0.1643
$M_{0,Fr}$ with $n_S i$	36	4	9	1.28	0.2768
C_{Si_i} with $n_S i$	0.9	4	0.2	0.03	0.998
Error	45337.3	6431	7		
Total	200909.3	6559			

Table B.14: Summary of F and p values for ANOVA tests on 8-variable factorial experiment: External Silicon data

Variable	F	p	F	p	F	p	F	p
C_E	3316.4	0			362.25	0	430.84	0
β	83.15	0	24.16	0	254.96	0	2737.77	0
P_{max}	375.8	0	109.12	0	600.52	0	4490.95	0
T_1	5.46	0.0043	1.59	0.2048	7089.18	0	53965.19	0
$k_{E,Pr}$	22.9	0	6.63	0.0013	356.29	0	2028.16	0
$M_{0,Fr}$	1774.26	0	514.77	0	291.05	0	112.39	0
C_{Si_i}	1.54	0.2138	0.45	0.6361	33.3	0	98.94	0
$n_S i$	0.14	0.8657	0.04	0.9591	278.86	0	1762.09	0
C_E with β	96.61	0			9.66	0	2.89	0.0555
C_E with P_{max}	321.83	0			25.66	0	7.65	0.0005
C_E with T_1	70.43	0			15.82	0	246.46	0
C_E with $k_{E,Pr}$	13	0			24.61	0	275.85	0
C_E with $M_{0,Fr}$	1793.94	0			233.66	0	3.23	0.0397
C_E with C_{Si_i}	2.27	0.0596			5.2	0.0004	2.9	0.055
C_E with $n_S i$	1.72	0.1415			3.3	0.0104	2.95	0.0525
β with P_{max}	86.06	0	24.99	0	233.63	0	1894.32	0
β with T_1	1.74	0.1375	0.5	0.7325	40.99	0	567.64	0
β with $k_{E,Pr}$	1.89	0.1097	0.54	0.7045	19.02	0	104.61	0
β with $M_{0,Fr}$	142.6	0	41.36	0	3.49	0.0075	3.27	0.0111
β with C_{Si_i}	0.05	0.9946	0.02	0.9995	0.19	0.9442	3.1	0.0147
β with $n_S i$	0.18	0.9474	0.05	0.995	11.47	0	132.53	0
P_{max} with T_1	13.34	0	3.87	0.0039	113.5	0	745.66	0
P_{max} with $k_{E,Pr}$	2.57	0.0361	0.75	0.5603	12.94	0	125.66	0
P_{max} with $M_{0,Fr}$	116.11	0	33.67	0	10.53	0	9.69	0
P_{max} with C_{Si_i}	0.21	0.9324	0.06	0.9935	2.54	0.0382	9.3	0
P_{max} with $n_S i$	0.51	0.725	0.15	0.9623	34.33	0	262.16	0
T_1 with $k_{E,Pr}$	16.9	0	4.91	0.0006	176.71	0	1057.45	0
T_1 with $M_{0,Fr}$	36.61	0	10.62	0	2.8	0.0246	51.02	0
T_1 with C_{Si_i}	1.03	0.3904	0.3	0.88	17.48	0	47.36	0
T_1 with $n_S i$	0.02	0.9995	0	1	160.58	0	1041.44	0
$k_{E,Pr}$ with $M_{0,Fr}$	4.16	0.0023	1.21	0.3028	19.75	0	0.14	0.9694
$k_{E,Pr}$ with C_{Si_i}	0.17	0.9532	0.05	0.9955	0.28	0.894	0.13	0.9706
$k_{E,Pr}$ with $n_S i$	0.01	0.9996	0	1	9.97	0	63.17	0
$M_{0,Fr}$ with C_{Si_i}	1.63	0.1643	0.47	0.7585	1.44	0.2194	38.27	0
$M_{0,Fr}$ with $n_S i$	1.28	0.2768	0.37	0.8277	4.46	0.0013	80.01	0
C_{Si_i} with $n_S i$	0.03	0.998	0.01	0.9998	11.54	0	75.84	0

Table B.15: Comparison of model output to data from Experiment 1 in Pan et al. [59]. Model data is averaged for days 23 to 25. Error is absolute relative error.

	Total DA			Cellular DA			External Si		
Flow d^{-1}	Model	Data	Percent Error	Model	Data	Percent Error	Model	Data	Percent Error
0.2	48.6	50	2.8	0.607	0.53	16.7	36.8	29.5	24.7
0.3	20.4	27.8	26.6	0.290	0.27	7.4	51.9	46.0	12.7
0.4	8.89	11.1	19.9	0.146	0.17	14.1	66.7	62.3	6.6
0.5	3.58	5.56	35.6	0.076	0.8	5.0	80.2	79.1	1.4
0.6	0.909	2.78	67.0	0.025	0.06	58.3	97.8	95.6	2.3

Table B.16: Comparison of model output to data from Experiment 2 in Pan et al. [59]. Model data is averaged for days 28 to 30. Error is absolute relative error.

	Total DA			Cellular DA			External Si		
Flow d^{-1}	Model	Data	Percent Error	Model	Data	Percent Error	Model	Data	Percent Error
0.2	389	245	57.8	7.07	5.6	26.2	3.23	2.3	40.4
0.3	122	145	15.9	2.47	2.2	12.2	5.12	2.3	122
0.4	34.1	73	53.3	0.76	1.3	41.5	8.37	2.0	318

Table B.17: Model Parameter values for Chapters 4 and 5. Only parameters whose values are different than in Table B.4 are listed.

Parameter	Description	Ch 4	Ch 5
c_{si}	Proportionality constant for external Si	16.40e7	12.40e7
$n_{Si,e}$	Density of transport sites for Si uptake	2.115e3	4.815e3
λ_0	Maximum increase in uptake efficiency for Si	100.0	154.5
ρ	Decrease in uptake efficiency per unit external Si	0.7000	0.1800
S	Rate constant	1.160e-10	4.560e-10
P_{max}	Maximum photosynthetic rate	8.000e-3	2.800e-1
β	Photoinhibition index	4.800e-5	4.800e-5
C_{C_i}	Wait time for one molecule of C	2.000e-6	16.50e-6
$C_{N,i}$	Wait time for one molecule of N	2.000e-6	16.50e-6
C_{P_i}	Wait time for one molecule of P	2.000e-6	16.50e-6
C_{E_i}	Wait time for one molecule of ATP	2.000e-6	16.50e-6
C_{Si_i}	Wait time for one molecule of Si	2.000e-6	16.50e-6
$m_{0,Pr}$	Maximum number of protein molecules fixed per time	6.400e-7	6.400e-7
$m_{0,Ps}$	Maximum number of polysaccharide molecules fixed per time	4.800e-6	6.800e-6
$m_{0,Fr}$	Maximum number of frustule molecules fixed per time	7.300e-6	5.000e-6
$m_{0,DA}$	Maximum number of DA molecules fixed per time	2.100e-12	9.200e-12

Table B.18: Summary of results for DA production for varying N and Si levels

Si	N	Da production
Low	High	High
Low	Low	Low
High	High	Low
High	Low	Low

Vita

Maria Siopsis was born in Dennis, Massachusetts on August 1, 1972. She received her B.A. degree from Drew University in Madison, New Jersey in December, 1993 with a double major in Applied Mathematics and Spanish literature. She enrolled at the University of Tennessee in January 1994. Until Fall of 1995, she worked on an EPA project to model the Fort Loudoun Lake ecosystem with Dr. Thomas Hallam and several other graduate students. She then became a graduate teaching assistant in the Department of Mathematics where she taught Mathematics for the Biosciences. In January 1997, she joined a team of scientists at The Institute for Environemntal Modeling on a project to model systems in the Smoky Mountains. She worked closely with Dr. Roger Clapp on the hydrological modeling of the Bear Creek Watershed. Beginning in August 1999, she again served as a graduate teaching assistant for the Department of Mathematics, a position which she continued to hold until December, 2001. In August of 2001, she became an adjunct instructor of mathematics at Maryville College in Maryville Tennessee. For the Spring semester of 2002, she was visiting instructor of Mathematics at the same institution. She currently holds a tenure track position at Maryville College in the Division of Mathematics and Computer Science.